

A Corneal Anti-Fibrotic Switch Identified in Genetic and Pharmacological Deficiency of Vimentin

Paola Bargagna-Mohan¹, Riya R. Paranthan², Adel Hamza³, Chang-Guo Zhan³, Do-Min Lee³, Kyung Bo Kim³, Daniel L. Lau⁴, Cidambi Srinivasan⁵, Keiko Nakayama⁶, Keiichi I. Nakayama⁷, Harald Herrmann⁸, and Royce Mohan^{1*}

From the ¹Department of Neuroscience, University of Connecticut Health Center, Farmington, CT 06030

²Department of Ophthalmology & Visual Sciences, ³Department of Pharmaceutical Sciences, ⁴Department of Computer and Electrical Engineering, and ⁵Department of Statistics, University of Kentucky, Lexington, KY 40503

⁶Division of Developmental Genetics, Tohoku University Graduate School of Medicine, Sendai, Miyagi, 980-8575, Japan

⁷Department of Molecular and Cellular Biology, Medical Institute of Bioregulation, Kyushu University, Fukuoka 812-8582, Japan

⁸Functional Architecture of the Cell Group, German Cancer Research Center (DKFZ), D-69120 Heidelberg, Germany

Running title: *Vimentin is a Fibrosis Target*

*To whom correspondence should be addressed: Royce Mohan, PhD, John A. and Florence Mattern Solomon Endowed Chair in Vision Biology and Eye Diseases, Laboratory of Chemical Biology & Drug Discovery, Department of Neuroscience, University of Connecticut Health Center, 263 Farmington Ave, Farmington, CT 06030-3401. Tel: 860 679 2020; Fax: (860) 679 8766; E-mail: Mohan@UCHC.edu

Background: Withaferin A (WFA) is a vimentin-targeting inhibitor that has potent anti-proliferative activity.

Results: WFA protects against corneal fibrosis by downregulating injury-induced vimentin to exert epithelial cell cycle arrest and inhibit myofibroblast expression, which is a mechanism closely mimicked in vimentin-deficient mice during injury healing.

Conclusion: Vimentin is a novel fibrosis target.

Significance: Ocular fibrotic conditions that overexpress vimentin could be treatable with WFA.

SUMMARY

The type III intermediate filaments (IFs) are essential cytoskeletal elements of mechanosignal transduction and serve critical roles in tissue repair. Mice genetically deficient for the IF protein vimentin (*Vim*^{-/-}) have impaired wound healing from deficits in myofibroblast development. We report a surprising finding made in *Vim*^{-/-} mice that corneas are protected from fibrosis and instead promote regenerative healing after traumatic alkali injury. This reparative

phenotype in *Vim*^{-/-} corneas is strikingly recapitulated by the pharmacological agent withaferin A (WFA), a small molecule that binds to vimentin and downregulates its injury-induced expression. Attenuation of corneal fibrosis by WFA is mediated by downregulation of ubiquitin conjugating E3 ligase Skp2 and upregulation of cyclin-dependent kinase inhibitors (CKIs) p27^{Kip1} and p21^{Cip1}. In cell culture models, WFA exerts G2/M cell cycle arrest in a p27^{Kip1} and Skp2-dependent manner. Finally, by developing a highly sensitive imaging method to measure corneal opacity, we identify a novel role for desmin overexpression in corneal haze. We demonstrate that desmin downregulation by WFA via targeting the conserved WFA-ligand binding site shared among type III IFs promotes further improvement of corneal transparency without affecting CKI levels in *Vim*^{-/-} mice. This dissociates a direct role for desmin in corneal cell proliferation. Taken together, our findings illuminate a previously unappreciated pathogenic role for type III IF overexpression in corneal fibrotic conditions and

also validate WFA as a powerful drug lead towards anti-fibrosis therapeutic development.

Traumatic injury, in particular alkali burns to the eye, can cause irreversible loss of vision due to corneal opacification from fibrosis, which often necessitates corneal transplantation as a means of restoring vision. When coupled with the lack of effective therapeutic modalities and served by inadequate medical infrastructure, corneal rehabilitation for millions of people in underdeveloped nations remains a vital challenge (1). Reflecting this insidious enigma, the leading cause of worldwide blindness, second only to cataract, is from corneal pathology where fibrosis is a central binding mechanism of refractive failure. Corneal haze, considered a reversible form of refractive aberration is also a complication from corneal disease and injuries and also can present in 2 to 5% of subjects after surgical and laser vision corrective procedures (2). As procedures such as LASIK² (laser in situ keratomileusis) have become very popular crossing the 10 million people mark in the US alone, concerns over corneal failure to heal in patients who have had vision corrective surgery has also gained recent importance (3). Considering the unique requirement for transparency (4), the molecular underpinnings of how scar-free healing can be promoted to restore visual acuity continues to remain a vital challenge for corneal transplantation, rehabilitation and refractive surgery.

The type III intermediate filaments (IFs) are a family of highly homologous cytoskeleton proteins that are widely conserved from humans to cold-blooded fish (5). These proteins mechanically integrate external influences with cellular biochemical processes and govern many critical aspects of cell structure, cell division, cell differentiation, apoptosis and cell movement, acting together with the actin and microtubule cytoskeletal elements to regulate functions of a plethora of cellular proteins (6-8). These IFs are expressed widely, e.g. in mesenchymal cells such as fibroblasts, muscle and endothelial cells, elsewhere in leucocytes, and in astrocytes and macroglia of the central nervous system (CNS). The genetic knockouts of IFs while revealing that they are not essential for development or reproduction (9, 10), have drawn more recent attention to their functions in tissue repair and stress response (11, 12). Vimentin is the prototypic Type III IF protein that is widely studied because of its involvement in wound healing,

fibrosis, angiogenesis, tumor cell differentiation, migration and metastasis (13-18). Vimentin plays a critical role in wound repair by providing activated wound fibroblasts during transition to the myofibroblastic phenotype with force generation required for tissue contraction (19). Notwithstanding, vimentin-deficient (*Vim*^{-/-}) mice display deficits in physiological wound closure from delayed myofibroblast activation and defective collagen contraction (20), but these mice are otherwise physiologically normal (9). Vimentin expression in endothelial cells also helps to form anchoring structures to assist leukocyte extravasation from vasculature and hence *Vim*^{-/-} mice are severely compromised in leukocyte transmigration, which is important for immune activation during infection (21). Because vimentin is also the sole IF expressed in vascular endothelial cells, neovascularization responses in *Vim*^{-/-} mice are impaired (12, 16). Despite previous studies showing that vimentin is overexpressed in the cornea during injury and fibrosis (22, 23), its precise role in regulating corneal injury repair has remained largely unexplored.

The small molecule withaferin A (WFA) is a pluripotent natural product (24, 25), which was recently discovered to target vimentin (16). WFA covalently binds soluble tetrameric vimentin at its single cysteine residue that is present in the conserved rod 2B domain (16). Taking advantage of WFA's targeting this conserved cysteine residue found in type III IFs, we recently demonstrated that WFA, in addition to targeting vimentin in the retina, also binds to glial fibrillary acidic protein (GFAP) and downregulates GFAP expression in reactive Müller cells to block retinal gliosis (26, 27). Thus, expanding the broad clinical usefulness of this newly discovered type III IF targeting drug, others have also exploited vimentin's *in vivo* druggability by WFA to illustrate tumor blockade through downregulation of vimentin (15, 28), and as well to demonstrate protection against bacterial meningitis via vascular targeting of vimentin (15, 28). Here we report a novel finding using a mouse model of alkali injury that vimentin and the related IF desmin are coordinately overexpressed during corneal fibrosis. We advance an important discovery that *Vim*^{+/+} mice treated with WFA recapitulates several hallmark features of *Vim*^{-/-} mice in their protection from corneal fibrosis. Finally, we reveal a novel role for desmin in corneal refractive aberration, which we have unveiled in *Vim*^{-/-} mice that

demonstrate WFA's targeting of this second IF promotes further restoration of corneal transparency.

EXPERIMENTAL PROCEDURES

General methods- Withaferin A (WFA) was purchased from a commercial vendor (Chromadex, Santa Ana, CA) and WFA-Bt synthesis has been previously described (29). All animal experiments were conducted in accordance with the Declaration of Helsinki, and procedures approved by IACUC committees of the University of Kentucky and University of Connecticut Health Center.

Cell culture- Wild-type, *Skp2*^{-/-}, and *p27*^{-/-} Mouse Embryonic Fibroblasts (MEFs) were cultured in DMEM medium containing 10% FBS, 100 mM sodium pyruvate, 10 mM non-essential amino acids, 200 mM L-glutamine, and 50 mM β -mercaptoethanol as previously described (30) and used before passage 5. Corneal fibroblasts were derived from primary cultures of keratocytes isolated from corneas of New Zealand white rabbits by collagenase digestion and cultured in MEM medium containing 10% FBS and penicillin and streptomycin (100U/ml) as previously described (31). Cells were used before passage 8.

Three-dimensional Model of the Human Desmin Tetramer Fragment- The homology modeling of the desmin 3D tetramer model and molecular docking for the WFA ligand binding was carried out essentially as previously described (16).

Cell Cycle Analysis- MEFs from wild-type mice and *p27*^{Kip1}^{-/-} and *Skp2*^{-/-} were grown to confluence, growth arrested by serum starvation for 48 h and treated with vehicle or WFA in presence of serum for 21 h for cell cycle analysis as previously described (24).

In vivo Corneal Injury Model- The corneal alkali injury model in *Vim*^{-/-} and *Vim*^{+/+} in 129 Svej background has been described in detail previously (16). Injured mice were treated with vehicle (DMSO) or WFA (2 mg/kg solubilized in DMSO) on the day of injury and every subsequent day by intraperitoneal injection for a period of 7 or 14 days.

Immunofluorescence- Using procedures previously described (16), whole- eye sections from *Vim*^{+/+} and *Vim*^{-/-} mice were prepared by cryosectioning. Slides were probed with the following primary antibodies, diluted in a background-reducing buffer (Dako North America, CA): anti-rabbit vimentin (Abcam, 1:200), anti-mouse desmin (Dako, 1:200), anti-mouse α -SMA (Dako, 1:100), anti-mouse *Skp2* (Abcam, 1:50), anti-rabbit *p27*^{Kip1} (Santa Cruz

Biotechnology, Inc., 1:50), anti-rabbit vimentin (H-84, Santa Cruz Biotechnology, Inc., 1:100), anti-rat monoclonal E-cadherin (Abcam, 1:1000) and anti-rabbit TGF- β 2 (Santa Cruz Biotechnology, Inc., 1:50) overnight at 4°C. After washing, sections were probed with respective secondary antibodies conjugated to Alexa Fluor 488 or 545 (Invitrogen) for 45 min at room temperature and counterstained with 4,6-diamidino-2-phenylindole (DAPI, 1mg/mL in 0.1 M PBS) for 10 minutes. Digital images were acquired on a Nikon TE2000 microscope at 30X magnification and as well on Olympus IX81 fluorescence microscope equipped with MetaMorph software. Images were assembled using Adobe Photoshop Software. For vimentin tissue staining, samples were washed more extensively (30 h) at 4°C to improve the quality and resolution of specific staining in fibroblasts from injured corneas due to very high expression of antigen. Thus, uninjured control samples processed in parallel required a lower threshold setting for imaging due to their relatively low levels of vimentin. In related studies, deconvolution software (MetaMorph) was also employed to assess the filamentous staining of vimentin in corneal sections. The measurement of activated p65/Rel A was assessed by its nuclear localization, which was scored by counting the numbers of nuclei (DAPI staining) in the epithelium from representative tissue sections of each treatment group (n=8) that showed also nuclear co-staining with antibody to p65/RelA. The data was graphed as the percent of epithelial cells showing nuclear-localized p65/RelA positive expression.

TGF- β treatment- *Vim*^{+/+} and *Vim*^{-/-} fibroblasts (16) were cultured at low density (40% confluence) in 8-well chamber slides (Nalgene, Nunc, NY). After cell attachment, cell cultures in triplicate wells were incubated in media containing 0.2% serum alone, or with serum plus 5 ng/ml TGF- β 1 (R&D systems, MN) in the presence of vehicle (DMSO) or 500 nM WFA. The medium with each of these treatments was replaced every 2 days for a treatment period of 6 days. Cells were fixed in methanol and processed for immunostaining for α -SMA expression. Representative frames from triplicate experimental samples were assessed for numbers of cells positive for α -SMA staining. DAPI counter staining was employed to provide a total count of cells in each frame.

Immunoblotting of Protein Extracts- Corneal full-thickness buttons were minced in ice-cold lysis buffer (5 mM NaF, 1 mM PMSF, 1 mM DTT, 20 mM HEPES pH 7.5, 1 mM EDTA, 400 mM NaCl, 1mM EGTA, 0.1% NP-40) to which was added protease inhibitor cocktail (Roche). Sodium dodecylsulfate (SDS) was subsequently added to a final concentration of 2% (w/v) and lysates were flash-frozen and thawed 3 times, passed through a G-25 syringe needle multiple times, vortexed and finally centrifuged for 10 min at 14,000 rpm to sediment debris. The supernatant representing total proteins was collected and equal amount of protein (Bio-Rad protein assay; Bio-Rad) was fractionated by SDS-polyacrylamide gel electrophoresis. For IF-poor (detergent-soluble) protein extractions, corneal tissue was extracted using a modified lysis buffer (5 mM NaF, 1 mM PMSF, 50 mM Tris pH 7.5, 1 mM EDTA, 150 mM NaCl, 1% NP-40) to which was added protease inhibitor cocktail (Roche). The supernatant representing soluble proteins after centrifugation was adjusted with SDS-Laemmli sample buffer prior to SDS-PAGE analysis. Western blotting as performed as previously described (16). Protein blots were probed with anti-mouse desmin (Dako, 1:400), anti-mouse α -SMA (Dako, 1:400), anti-rabbit Vimentin (V9, Santa Cruz Biotechnology, Inc., 1:400), anti-mouse Skp2 (Santa Cruz Biotechnology, Inc., 1:200), anti-mouse p27^{Kip1} (Santa Cruz Biotechnology, Inc., 1:200), anti-mouse p21^{Cip1} (Santa Cruz Biotechnology, Inc., 1: 100), anti-rabbit cyclin E (Abcam, 1:200), anti-rabbit TKT (1:1000, a gift from Dr. Joram Piatigorsky (National Eye Institute/NIH), anti-annexin II (H50, Santa Cruz Biotechnology, Inc., 1:200), anti-rabbit β -actin (Abcam, 1:1000), and anti-GAPDH (Santa Cruz Biotechnology, Inc., 1:1000). Blots were reprobed as described previously (16, 26). Blots were scanned and band intensities quantified using NIH ImageJ software and normalized to GAPDH or β -actin levels.

Tissue fixation and transmission electron microscopy – Corneas from two representative mice per group were used. Corneas were collected immediately after mouse sacrifice, fixed immediately in 3.5% glutaraldehyde/4% paraformaldehyde in 0.1 M cacodylate buffer, pH 7.2 for 1.5 hours at 4° C by immersion. Tissue pieces cut in fixative, then washed in 0.1 M cacodylate with 5% sucrose four times for 15 min each and post fixed with 1% OsO₄ in buffer for 1.5 hours at 4° C. After washing in 0.1M cacodylate buffer they were dehydrated in graded

manner in ethanol (from 50% through 100%) at 4^oC, followed by final incubation in absolute ethanol at room temperature. Tissues were placed in propylene oxide at room temp for 30 min, followed by infiltration with 50% Epon Araldite w/ accelerator-50% propylene oxide overnight. The propylene oxide-resin mixture was poured off and tissue placed in fresh 100% resin for 2 hours. Tissues were embedded in beam capsules for 48 hours at 60° C. Thin sections (70-80 nm) were obtained on a Reichert Ultracut E microtome and examined on a Philips Tecnai Biotwin 12 transmission electron microscope. Representative images from 35 to 50 frames/cornea were collected for analysis. A second set of corneal embedded sections were cut on a Leica UC7 ultramicrotome, mounted on 200 mesh Cu/Rh grids and stained with 6% Methanolic Uranyl Acetate for 4 min and Sato's Lead for 4 min and examined on a Hitachi H-7650 transmission electron microscope.

Isolation of WFA-Bt-binding proteins by affinity chromatography- The WFA-Bt ligand binding studies in early passage (passage between 5 and 6) rabbit corneal fibroblasts was performed as previously reported for endothelial cells and astrocytes (16, 26). In brief, fibroblast cultures plated at 60 to 70% confluency were incubated with 5 μ M WFA or vehicle for 30 min. WFA-Bt (5 μ M) was subsequently added to the medium and cells incubated for 2 h. Protein extracts were prepared in buffer A (5 mM Tris pH 7.6, 50 mM NaF, 1% Triton X-100, 5 mM EGTA) supplemented with a proteinase inhibitor cocktail (Roche). Equal amount of proteins were precleared on agarose beads (Sigma) to remove nonspecific binding proteins. The beads were then centrifuged and precleared cell lysates were repeatedly loaded three times on columns containing NeutrAvidin-agarose beads (Pierce) to maximize immobilization of biotinylated proteins. After extensive washing with ice-cold loading buffer A, bound biotinylated proteins were eluted in Laemmli gel loading buffer containing β -mercaptoethanol, and subjected to SDS-PAGE on 10% polyacrylamide gels and transferred to PVDF membrane for western blot analysis. Blots were probed with anti-mouse vimentin (V9, Santa Cruz Biotechnology, Inc., 1:400), and anti-rabbit annexin II (H50, Santa Cruz Biotechnology, Inc., 1:200).

WFA ligand binding studies with recombinant tetrameric desmin and Liquid Chromatography-Mass Spectrometric (LC-MS) Analysis - Binding studies with WFA was done essentially as described before

for vimentin (16) and GFAP (26). Briefly, purified soluble recombinant human desmin (32) was incubated with vehicle or 5 μ M WFA for 1 h at 37°C. Protein samples were subjected to tryptic digestion and LC-ESI-MS-MS analysis was performed on a ThermoFinnigan LTQ linear ion trap mass spectrometer (ThermoFinnigan, San Jose, CA). Resulting MS-MS spectra were searched against proteins in the Swiss-Prot database with the X!Tandem search engine (www.thegpm.org). The assignment of fragment ions in the MS-MS of the modified and unmodified peptides was obtained with the X!Tandem protein database search engine allowing for a variable modification of +470 Da for the WFA adduct.

Statistical Analysis- The statistical analysis to compare the percentile curves of the clarity data employed three different but related non-parametric test procedure (Kolmogorov-Smirnov test, Cramer-von Mises test, and Kuiper's test). All three procedures lead to the same conclusion with P-values agreeing up to 4-digits. The computations were performed using SAS version 9.2.

RESULTS

Corneal fibrotic switch is blocked by genetic and pharmacological deficiency of vimentin

Several independent experiments described here and in following sections indicate that the corneal fibrotic switch can be attenuated by causation of vimentin deficiency. Exploiting the modified alkali injury model (33) we show in injured corneas of *Vim*^{+/+} mice that by post-injury day14 (d14) corneal transparency is lost due to heightened fibrosis (Fig. 1A). Surprisingly, in *Vim*^{-/-} mice subjected in parallel to alkali injury there is remarkable improvement in corneal healing and these mice regain very significant levels of corneal transparency (Fig 1A- right panel). We were prompted to ask whether use of a complementary approach to pharmacologically downregulate vimentin would mimic the phenotype of genetic deficiency of vimentin. We exploited the vimentin-targeting small molecule WFA (16, 26) and show that in d14 injured *Vim*^{+/+} mice treatment with 2 mg/kg WFA significantly restored corneal clarity to the extent similar to that observed in d14 healing *Vim*^{-/-} mice (Fig. 1A, B). In comparison, WFA effects on *Vim*^{-/-} mice at d14 promoted similar levels of healing as that of vehicle-treated *Vim*^{-/-} mice (Fig. 1B). To address whether this novel corneal reparative healing mechanism exerted in vimentin deficiency was

recapitulated due to WFA's efficacy to reduce injury-induced vimentin we analyzed corneal tissues first by western blot analysis (Fig. 1C). We show that injury-induced vimentin expression by d7 in *Vim*^{+/+} corneas was potently inhibited by WFA treatment. This WFA targeting activity is specific to type III IFs, as annexin II, an unrelated cytoskeletal-associated protein reported also to bind WFA in cancer cells (34), was not downregulated by drug treatment (Fig. 1D). Our findings were further corroborated by immunohistochemical analysis that showed injury-induced expression of vimentin occurs in both corneal epithelium and in stromal cells, which was potently downregulated by WFA at d7. Corneas of d14 *Vim*^{+/+} mice expressed higher levels of vimentin than at d7, and again, WFA potently downregulated vimentin in both epithelium and stroma (Fig. 1E). To clarify whether vimentin-overexpressing stromal fibroblasts had invaded the epithelium we also co-stained corneal sections with the epithelial marker E-cadherin. There were a remarkable number of filamentous vimentin-positive stromal cells found to have invaded the corneal epithelium at sites showing discontinuity of E-cadherin staining. Corneas from WFA-treated *Vim*^{+/+} mice at d14 revealed an absence of this phenotype, and stromal expression of vimentin was also greatly reduced (Supplemental Fig. S1). Next, we investigated whether vimentin downregulation is due to direct covalent binding by WFA, as previous findings we made in vascular endothelial cells and brain astrocytes showed that soluble tetrameric vimentin is targeted (16, 26). Employing a cell culture model we differentiated naïve primary cultures of corneal keratocytes to fibroblasts (35) and performed *in vivo* ligand binding studies to identify WFA's target(s). Cells were incubated with the cell permeable biotinylated WFA analog (WFA-bt) in the presence and absence of free-unconjugated WFA and soluble proteins were affinity isolated by streptavidin chromatography, boiled in 2-mercaptoethanol Laemmli buffer and fractionated by gel electrophoresis (26, 29). Gel blots when probed sequentially with vimentin and annexin II antibody revealed that WFA-bt only formed a covalent adduct with vimentin, but not with annexin II, and this binding was competed *in vivo* by excess WFA (Fig. 1F). Taken together, our findings corroborate that the *in vivo* pharmacological downregulation of injury-induced vimentin by WFA that affords protection against corneal fibrosis, a phenotype that we show is corroborated in genetic deficiency of vimentin.

Corneal myfibroblast and TGF- β activation is attenuated by vimentin deficiency

Myofibroblast activation through acquisition of α -SMA expression in wound fibroblasts is considered a major phenotypic switch that drives corneal fibrosis (36). Also in our alkali burn model, α -SMA expression is upregulated in the stromal cells of injured *Vim*^{+/+} mice (Fig. 2A) and its increased expression is time dependent, reaching high levels at d14 (Fig. 2A). WFA significantly down regulates α -SMA expression, being especially effective at d14 (Fig. 2A). Interestingly, injured *Vim*^{-/-} corneas also showed early increased production of α -SMA at d7, however, this induced expression is not sustained and became devoid of detectable α -SMA expression by d14 in both vehicle and WFA-treated *Vim*^{-/-} samples (Fig. 2B). Western blot analysis confirmed the staining results showing complete downregulation of α -SMA expression in *Vim*^{-/-} corneas at d14 (Fig. 2C, D).

Given the well-documented role for TGF- β in corneal fibrosis as a stimulator of myofibroblast transformation and mediator of α -SMA expression (36, 37), we next investigated TGF- β expression levels in injured *Vim*^{+/+} and *Vim*^{-/-} corneas. We found that TGF- β was appreciably increased in the epithelium and stroma of injured- *Vim*^{+/+} cornea and WFA treatment potently downregulates its expression to level similar to the uninjured cornea (Fig. 3A). WFA treatment also potently reduced TGF- β expression in *Vim*^{+/+} corneas (Fig. 3A). On the contrary, in d14 injured *Vim*^{-/-} mouse corneas low levels of TGF- β was found in the epithelium and largely undetected in the corneal stroma (Fig. 3A). This epithelial low expression pattern was maintained in *Vim*^{-/-} mice treated with WFA. To learn whether vimentin expression is necessary for TGF- β regulation, fibroblasts from *Vim*^{+/+} and *Vim*^{-/-} mice were investigated. We found that *Vim*^{+/+} cells stimulated with TGF- β induced α -SMA expression by 25-fold over control, which was reduced significantly by WFA down to 5-fold over controls (Fig. 3B, C; $P < 0.05$). On the contrary, *Vim*^{-/-} cells responded weakly to TGF- β resulting in only 1.3-fold mean increased expression of α -SMA ($P = 0.0171$) and WFA's antagonism of this induction was not significant ($P = 0.1586$). Thus, we were curious whether recovery of corneas from fibrotic injury displayed other biomarkers associated with

transparency, such as maintenance of tissue transketolase (TKT) (38). Western blot analysis revealed that TKT expression in d14 injured *Vim*^{+/+} corneas was reduced by 7-fold from the levels found in uninjured corneas and WFA treatment restored TKT expression to levels almost that of controls. In *Vim*^{-/-} corneas injury resulted in only 40% reduction of TKT expression compared to uninjured controls and WFA did not produce any change (Fig. 3D, E). To further compare the healing characteristics of *Vim*^{+/+} and *Vim*^{-/-} corneas we investigated their ultrastructure by transmission electron microscopy (TEM) (Fig. 3F). Corneas from d14 *Vim*^{+/+} mice showed the increased presence of myofibroblasts that revealed extensive rough endoplasmic reticuli and enlarged cytoplasm (Fig. 3F, a), whereas the samples from uninjured *Vim*^{+/+} corneas showed scant rough endoplasmic reticuli characteristic of normal corneal keratocytes (Fig 3F, c). We also found polymorphonuclear neutrophils (PMNs) in injured *Vim*^{+/+} corneas (Fig 3F, b). WFA treatment also reduced the numbers of PMNs detected. Monocytes/macrophages were rarely detected at d14 in *Vim*^{+/+} corneas (data not shown), which suggests that the CD11b⁺ cells detected by immunostaining are mostly PMNs. Comparison of the fibrillary structure of collagen and fibril spacing in uninjured *Vim*^{+/+} and *Vim*^{-/-} mice showed no remarkable differences (data not shown). Importantly, corneal epithelium in injured *Vim*^{+/+} mice at d14 was often observed to be thin and remarkably conjunctivalized as shown by significant numbers of goblet cells (Supplemental Fig. S2). In comparison, the epithelium of injured *Vim*^{-/-} mice had acquired corneal cell characteristics similar to that of uninjured mice, which was similar also after WFA treatment in injured *Vim*^{+/+} and *Vim*^{-/-} mice at d14 (Supplemental Fig. S2). Collectively, these findings reveal a critical role for vimentin in myofibroblast activation that enables the corneal fibrotic switch to occur, which can be pharmacologically attenuated by WFA or impaired when vimentin is absent. Thus, vimentin deficiency results in both restoration of corneal epithelial characteristics and stromal healing.

Vimentin expression supports inflammatory cell recruitment in injured corneas

Alkali injury to the cornea induces an inflammatory cascade driven by NF- κ B transcription factor activation where its pharmacological inhibition has been shown to also improve corneal burn

recovery in mice (39). We enquired whether WFA's *in vivo* efficacy on corneal injury is likewise also due to WFA's potent NF- κ B inhibitory activity (24, 40) that is potentially mediated by vimentin. Injured *Vim*^{+/+} corneas assessed at d7 showed reduction of I κ B- α levels, whereas *Vim*^{+/+} and *Vim*^{-/-} mice treated with WFA as well as vehicle-treated *Vim*^{-/-} mice exhibited restoration of I κ B- α in their corneas to ~75% of the levels that were found in uninjured tissues (Fig. 4A, B). These results were further confirmed by immunostaining corneal tissues at d14 where we found p65/RelA was nuclear localized in injured *Vim*^{+/+} corneas, whereas p65/RelA expression in all other injured corneas was found to be mostly cytoplasmic (Fig. 4C). Quantification of nuclear expression of p65/RelA in epithelium (overlap with DAPI, data not shown) revealed 20-fold induction in injured *Vim*^{+/+} corneas over uninjured corneas ($P < 0.0001$), which was reduced to 4-fold by WFA treatment ($P < 0.0001$). Injury to *Vim*^{-/-} corneas produced only a 4-fold induction over uninjured corneas ($P < 0.001$), and this induced nuclear expression was not altered by WFA activity ($P = 0.2295$) (Fig. 4D). These data provide evidence that vimentin regulates NF- κ B activation in the alkali injury model.

Alkali injury induces inflammation through recruitment of monocyte/macrophages and neutrophils that infiltrate into corneas, where increased numbers of CD11b⁺ neutrophils were associated with corneal opacity (41). We assessed corneas of *Vim*^{+/+} and *Vim*^{-/-} mice at d14 (Fig. 4E) that is the peak period of inflammatory cell infiltration in this model (42). Alkali injury significantly increased CD11b⁺ cell numbers in *Vim*^{+/+} corneas compared to *Vim*^{-/-} corneas showing 32-fold ($P = 0.0015$) versus 10-fold ($P = 0.01004$) increase, respectively. WFA treatment reduced the numbers of CD11b⁺ cells infiltrating the injured corneas producing a 4.2-fold increase ($P = 0.002525$) in *Vim*^{+/+} versus a 2.2-fold increase ($P = 0.005387$) in *Vim*^{-/-} corneas compared to their respective uninjured controls (Fig. 4F). This suggested that although vimentin deficiency significantly reduced the numbers of CD11b⁺ cells, WFA treatment in combination with vimentin deficiency resulted in the most potent inhibition of CD11b⁺ cell infiltration. Our result corroborates previous findings showing deficiency in type III IFs severely attenuate CD11b⁺ infiltration into injured

tissues of mice as revealed in the retinal detachment model (43).

Corneal epithelial expression of p27^{Kip1} is restored by genetic and pharmacological downregulation of vimentin

We next investigated whether the critical determinants of corneal healing is due to altered cell proliferation characteristics that is different between *Vim*^{+/+} and *Vim*^{-/-} mice. The CKI p27^{Kip1} is critically implicated in regulation of epithelial regeneration in the injury-healing cornea (44, 45). We show by western blots that p27^{Kip1} is potently downregulated by injury at d7 and d14 in *Vim*^{+/+} corneas. WFA treatment at d7 and d14 restored p27^{Kip1} to levels similar to that of uninjured mice (Fig. 5 A, B, C, D). p27^{Kip1} expression levels were also reduced at d7 in *Vim*^{-/-} corneas, and restored to near normal levels by WFA treatment (Fig. 5 A, B). However, at d14, the expression of p27^{Kip1} differed between the two mouse lines; in the injured *Vim*^{+/+} corneas p27^{Kip1} expression was persistently downregulated and WFA restored its expression back up levels found in uninjured corneas (Fig. 5 C, D). On the other hand, in the injured *Vim*^{-/-} corneas p27^{Kip1} expression was fully recovered and WFA treatment did not further alter its expression (Fig. 5 C, D). Immunostaining of tissues at d7 and d14 confirmed that nuclear-associated changes in p27^{Kip1} expression (overlap with DAPI staining; data not shown) were responsible for the alterations in protein analyzed by western blotting, and importantly, that induced p27^{Kip1} expression was predominantly occurring at the basal cell layer of the epithelium, which is the site of mitosis (Fig. 5G) (46). Since p27^{Kip1} expression is tightly controlled through the ubiquitin proteasome pathway via the activity of E3 ubiquitin ligase Skp2 (30), we investigated next the expression of Skp2's other cell cycle targets by western blotting. The CKI p21^{Cip1} was expressed at low levels in uninjured corneas and became nearly undetectable in injured *Vim*^{+/+} corneas at d14. WFA induced p21^{Cip1} expression by over 13-fold in d14 *Vim*^{+/+} healing corneas (Fig. 5C, D). Interestingly, uninjured corneas of *Vim*^{-/-} mice expressed 3.4-fold higher levels of p21^{Cip1} compared to uninjured *Vim*^{+/+} corneas. Consequently, in injured *Vim*^{-/-} corneas p21^{Cip1} levels declined by 7.5-fold and WFA treatment did not alter this expression level. On the other hand, in *Vim*^{+/+} corneas, cyclin E expression was expressed at high basal levels in uninjured tissue and downregulated by injury (Fig. 5C, D). This

expression was restored by WFA to levels almost reaching that of uninjured corneas in *Vim*^{+/+} mice. However, in injured *Vim*^{-/-} corneas cyclin E was highly downregulated with injury and remained downregulated even after WFA treatment (Fig. 5C, D). Finally, we investigated whether expression levels of Skp2 were also affected by WFA activity. Skp2 expression was highly induced in injured corneas of *Vim*^{+/+} mice and WFA treatment potently downregulated Skp2 expression to levels found in uninjured corneas (Fig. 5E, F). There was a similar level of injury-induced expression of Skp2 in *Vim*^{-/-} corneas at d14, however, WFA treatment reduced Skp2 expression by less than 50%. Taken together, these findings reveal that Skp2 expression is induced with injury in both *Vim*^{+/+} and *Vim*^{-/-} corneas, but its downregulation by WFA activity that is partly enabled in vimentin deficiency does not result in control of its targets p27^{Kip1}, p21^{Cip1} and cyclin E in *Vim*^{-/-} corneas.

Since Skp2 deficiency causes sustained expression of p27^{Kip1} that results in decreased corneal epithelial cell proliferation (44), we next investigated whether WFA's growth inhibitory activity was dependent on the Skp2-p27 axis. We exploited a cell culture model using mouse embryonic fibroblasts (MEFs) from wild-type and Skp2- and p27^{Kip1}-deficient mice (30). WFA induced potent G2/M cell cycle arrest in a dose-related manner in wild-type MEFs, but Skp2- and p27^{Kip1}-deficient MEFs completely lose this growth inhibition at both low and high concentrations of WFA (Fig 5H). Taken together, consistent with the major role of Skp2 to cause p27^{Kip1} degradation during G2-M progression (47), our findings identify the critical importance of Skp2-p27^{Kip1} axis in WFA's cell cycle targeting affects.

A reverse chemical genetic approach identifies desmin as a second binding target of WFA

Type III IFs are highly homologous and share as much as 62% overall amino acid identity (32). Since WFA covalently binds to the highly conserved rod 2B domain of tetrameric vimentin (16) and the corresponding 2B domain of tetrameric GFAP (26), we postulated that WFA should similarly also bind to the third IF member, desmin, at its rod 2B region that is highly conserved with that of vimentin (16). Therefore, we developed a molecular model for the tetrameric 2B segment of desmin bound to WFA using the tetrameric A₂₂ orientation (48), which was

also used previously to develop molecular models for vimentin (16) and GFAP (26). Stable binding of WFA in the ligand-binding pocket of tetrameric desmin, i.e. between the antiparallel half-staggered coiled-coil dimers, was revealed by docking analysis of the molecular dynamics (MD) simulated human desmin-WFA complex (Fig. 6). As shown with the vimentin-WFA and GFAP-WFA complexes (16), the invariant cysteine amino acid residue (Cys333) in the desmin helix lies in close proximity to the C3 and C6 carbons of WFA (Fig. 6A), which facilitates a proper orientation for nucleophilic attack by C333 on the electrophilic carbon centers of WFA (Fig. 6B). Having also identical residues in desmin that make contact with the ligand, Gln329 can form a hydrogen bond with the C1-carbonyl group of WFA and Asp336 can hydrogen bond with the C4-hydroxyl group of WFA. Therefore, we can superimpose the binding site of desmin-WFA on that of vimentin-WFA to reveal that the binding mode of WFA is near identical in both tetramer fragments (Fig. 6B). Sharing high degree of conservation in a region of 44 amino acids between vimentin and desmin, this segment of the 2B region bound by WFA has also 70.5% identical amino acids and 84% similarity (Supplemental Fig. S3). Lastly, the molecular mechanics/Poisson-Boltzmann surface area-calculated binding energies for the two complexes are found to be $\Delta G_{\text{bind}} \sim -17.3$ and -17.4 kcal/mol for vimentin-WFA and desmin-WFA, respectively. To validate this molecular model, we also performed *in vitro* binding analysis with purified human recombinant tetrameric desmin and WFA. Mass spectrometric sequencing analysis of tryptic peptides showed that WFA binds covalently at the predicted Cys333 residue, which was revealed by the addition of WFA's molecular mass to this amino acid residue (Supplemental Fig. S4), and this data is in agreement with our previous findings for vimentin and GFAP (16, 26).

WFA targets desmin expression in vivo

We next investigated by immunohistochemical analysis whether desmin might be upregulated during corneal fibrosis and thus become a potential target for WFA. Uninjured corneas did not show expression of desmin. In injured *Vim*^{+/+} corneas desmin IFs were found overexpressed in conjunctivalized epithelium and stroma at d7 and this expression pattern was potently downregulated by WFA treatment (Fig. 7A). Contrary to its abundant expression in injured *Vim*^{+/+}

corneas, desmin IF-expression in *Vim*^{-/-} corneas at d7 was barely apparent in the stroma (Fig 7B). WFA treatment potentially downregulated desmin also in *Vim*^{-/-} corneas at d7 to levels that became undetectable. Desmin IF staining was increased in the corneas of injured *Vim*^{+/+} mice at d14 being strongly expressed in the anterior stroma and sub-epithelial region, which was potentially downregulated by WFA. Remarkably, in *Vim*^{-/-} corneas desmin IF staining became more strongly expressed in the stroma at d14 and lower levels of expression in the epithelium was noted as dots (Fig. 7B, inset). WFA treatment downregulated desmin staining in the stroma, and only the epithelium showed increased dot-like nuclear-associated staining pattern suggesting IF polymer disassembly. As the tissue staining for desmin reveals almost exclusively the abundant polymeric structures of this protein in that the less abundant soluble forms are undetected, we also performed western blotting experiments to assess WFA's effects on total and soluble desmin expression. Low levels of total desmin expression was observed as a doublet band in uninjured *Vim*^{+/+} corneas representing mural cells of preexisting limbal blood vessels. However, *Vim*^{+/+} corneas at d7 and d14 showed presence of multiple bands indicating different desmin isoforms or post-translationally-processed variants. Injured *Vim*^{+/+} corneas also showed the greatest abundance (between 4-to-8-fold increase) and number of desmin species including a prominent 52-kDa upper band most prominently increased at d14 (Fig. 7C,D). WFA treatment potentially abrogated expression of these desmin bands at d7, and also caused quantitative changes in the abundance of lower molecular weight species at d14 (Fig. 7D). On the other hand, *Vim*^{-/-} uninjured corneas expressed similar low levels of the two desmin variants as found in d7 corneas, and these desmin variants became increased by 2-fold at d14. Interestingly, the protein band profile of desmin variants in *Vim*^{+/+} mice treated with WFA showed a similar pattern to that of vehicle-treated *Vim*^{-/-} corneas at d14, revealing also the striking absence of the prominent 52-kDa disease-associated desmin species. On the other hand, WFA-treated *Vim*^{-/-} corneas at d14 revealed a single desmin variant/species that likely derives from the desmin dots observed in the epithelium. As previous findings showed that WFA targets soluble tetrameric vimentin and GFAP that results ultimately in their insoluble forms being depolymerized *in vivo* (16, 26), we next investigated whether soluble desmin was targeted by WFA *in vivo*. Soluble (low salt extracted) proteins

(26) were isolated and western blotted for desmin. The injury-induced soluble desmin isoform (52 kDa band) was most strikingly reduced by WFA in d14 *Vim*^{+/+} corneas, whereas in *Vim*^{-/-} d14 corneas both injury-induced soluble desmin bands were downregulated by WFA (Fig. 7E, F). Collectively, these findings reveal that desmin is differentially regulated in injured *Vim*^{+/+} compared with *Vim*^{-/-} corneas, and furthermore, in vimentin deficiency WFA potentially targets injury-induced soluble desmin expression resulting in IF disassembly.

Desmin targeting attenuates corneal haze in vimentin deficiency

Finally, we wondered whether WFA's targeting of desmin in vimentin deficiency produced an effect on the quality of corneal repair beyond the noticeable attenuation of corneal fibrosis. We hypothesized that overexpression of desmin in *Vim*^{-/-} corneas at d14 could potentially alter refractive functions of the cornea via expression in wound fibroblasts. To afford a sensitive and objective quantitative method to measure corneal clarity in mice we developed a computer-based algorithm to assess level of corneal transparency. Slit-lamp biomicroscopy affords visualization of iris structural details enabling the examiner to score corneal transparency, thus, we premised that detection of pigment color of the iris using a digital method (49) could also be adopted as a surrogate measure of corneal transparency. Consequently, opacity from injury-induced fibrosis or haze that causes the cornea to whiten should alter the color spectrum captured in digital images. According to principles of color theory, white light is composed of equal representation of red, green and blue (Supplemental Fig. S5), and therefore, corneal opacity that renders the cornea white in color represents a deviation from the equal mixing of red, green and blue. The advantage of this color detection method is its digital sensitivity and that color interpretation is not left to human subjectivity (50). We coded the digital photographic images of mouse eyes and obtained in a blinded manner three representative equal sized rectangular segments (Fig. 8A) that were taken from non-overlapping regions of the cornea (avoiding the central pupil due to underlying lens). The image collection library was analyzed to measure deviation from the brown color baseline of uninjured eyes, which was valid because both *Vim*^{+/+} and *Vim*^{-/-} mice in 129 Svej strain have equivalent brown colored irises. The opacity values for injured vehicle-

and WFA-treated groups were plotted as a function of their percentile distributions (Fig. 8B), which revealed three important results. First, injured *Vim*^{+/+} corneas that ranked even in the top 10th percentile for clarity came only as close as the lowest 80th percentile group of injured *Vim*^{-/-} corneas (mean 1.47 versus 1.42, $P < 0.008$). This result confirmed our visual biomicroscopic assessment scoring data (Fig. 1B) that the *Vim*^{-/-} mice have a significant advantage over *Vim*^{+/+} mice for healing such corneal injuries (mean 1.09 versus 2.13, $P < 0.0001$). Second, vehicle-treated *Vim*^{-/-} mice showed a similar percentile rank distribution for corneal clarity as WFA-treated *Vim*^{+/+} mice (mean 2.04 versus 2.13, $P = 0.1704$), a finding also supported by visual scoring data revealing the pharmacological downregulation of vimentin had similar protective effects as genetic deficiency of vimentin. Lastly, and to our surprise, we found that restoration of corneal clarity was the greatest in *Vim*^{-/-} corneas when mice were treated with WFA (mean 2.13 versus 2.67, $P < 0.0001$). Statistical comparison of percentile distributions for human scored data and computer-assisted image analysis was also performed (Supplemental Table S1). This illustrated the greater sensitivity of the computer-assisted image method over human scored data. Taken together, we have identified vimentin as a major driver of the proliferative mechanism of corneal fibrosis and that the underlying haze observed in injured corneas of *Vim*^{-/-} mice is associated with overexpressed desmin. This desmin-related corneal haze that is also responsive to WFA treatment results in significant improvement of corneal clarity, which appears not to be directly associated with WFA's cell cycle regulatory mechanism.

DISCUSSION

The major finding of this study is that vimentin deficiency alters the fibrotic response to corneal alkali injury and instead engages a reparative healing mechanism to restore corneal clarity. We validate this novel discovery by complementing the genetic deficiency of vimentin with a pharmacological approach to cause vimentin downregulation, and thus, we also illuminate vimentin as a novel druggable target for potential treatment of fibrotic conditions.

A remarkable conclusion drawn from this study is that the pharmacological downregulation of vimentin by WFA in *Vim*^{+/+} mice broadly recapitulates the repair mechanism elicited in the genetic deficiency of vimentin in this corneal alkali injury model. In this

respect, we already have shown that vimentin deficiency impairs corneal neovascularization in this alkali injury model (16). Additionally, we recently reported that retinal gliosis manifested in response to corneal alkali burns was similarly attenuated in *Vim*^{-/-} mice and mediated by restoration of p27^{Kip1} expression in retinal ganglion astrocytes and glia, which mimicked the activity of WFA in the retina (26). Here, we identify that in addition to restoration of p27^{Kip1} expression in the healing corneal epithelium by WFA, the coordinate upregulation of p21^{Cip1} expression may be critical to the mechanism of corneal reparative healing elicited by vimentin downregulation. Considering that p27^{Kip1} null mice develop retinal gliosis and dysplasia even in absence of an injury (47, 51), whereas the corneas of these mice do not display ectopic or inappropriate epithelial proliferation even after corneal scrape injuries (44), this suggests that CKIs in addition to p27^{Kip1} may be important for corneal mitotic arrest. This rationale is supported by loss of corneal transparency in lumican-deficient mice that occurs, in part, through downregulated p21^{Cip1} expression, which causes aberrant cell proliferation (52). Taken together, our findings underscore that a novel vimentin-mediated negative regulation of CKI expression is associated with the corneal fibrotic switch in traumatic injury healing that is blocked by suppression of vimentin expression.

Vimentin is a motile protein that exists in many dynamic native states, most noted by its abundant filamentous structures that adorn the cytoplasm of mesenchymal cells (53). Soluble tetrameric vimentin (54), only a small fraction of cellular vimentin, undergoes annealing to form intermediate unit-length filaments (ULFs) that become rapidly incorporated into long polymeric forms (7, 55). As cells initiate G1 cell cycle phase, both protein synthesis of vimentin and its incorporation into polymers occurs (56). Investigating the cell cycle, we previously showed that WFA targets tetrameric vimentin *in vitro* and *in vivo* resulting in G0/G1 cell cycle arrest in endothelial cells and astrocytes (16, 26). We have also shown that the pool of soluble tetrameric vimentin becomes depleted in a WFA concentration-dependent manner, where at the higher concentrations of WFA filamentous vimentin collapse around the nucleus and ultimately their depolymerization was observed (16, 26). While it is still unclear how WFA-targeted soluble vimentin affects this dynamic process *in vivo*, phosphorylation-dependent mechanisms that govern

vimentin functions during cell cycle progression (57) may be affected by WFA (26). It is noteworthy that the dynamic reorganization of filamentous vimentin is also quite noticeable at prometaphase where granular dot-like structures believed to be depolymerized IFs become plentiful (58). This enriched pool of soluble vimentin might also be targeted by WFA during G2 cell cycle progression to cause mitotic arrest. Importantly, our findings also identify that both Skp2 and p27^{Kip1} are required for WFA's induction of G2/M cell cycle arrest as revealed in our study of MEFs from Skp2- and p27^{Kip1}-deficient mice. Corroborating this mechanism, downregulation Skp2 expression was also induced by a related natural product withanolide (59) that contains the conserved steroidal backbone and critical pharmacophore moieties of WFA (29) shown to be important for binding to the 2B region of type III IFs (16, 26). This growth inhibitory mechanism would be consistent with Skp2's expression becoming maximal at S and G2 phase (60), which also represents the critical time when p27^{Kip1} degradation by Skp2 occurs in G2 phase in order for progression into mitosis (47). Thus, identification that Skp2 and its target p27^{Kip1} are reciprocally responsive to WFA's activity in injured corneas of *Vim*^{+/+} mice, but not in *Vim*^{-/-} mice, links vimentin as a mediator of WFA's activity on the critical Skp2-p27^{Kip1} cell cycle axis. Furthermore, since p21^{Cip1} and cyclin E, other targets of Skp2's E3 ligase activity (30, 61) also responded to WFA activity in a vimentin-mediated manner during injury healing, it is clear that vimentin targeting can have profound regulatory control on many critical cell cycle regulators. This is obviously important to therapeutic development efforts that recognize suppressing Skp2 expression or interfering with its E3 ligase function has wide applications to diverse proliferative disorders and malignant conditions characterized by Skp2 overexpression (30, 62). Taken together, we believe that our findings illuminate vimentin as a novel druggable target for regulatory control over the critical Skp2-p27^{Kip1} axis and have also borne out WFA as an important chemical probe of this mechanism.

It is interesting that vimentin downregulation by WFA results in the differential regulation of p21^{Cip1} compared to p27^{Kip1}. This was noted in injured *Vim*^{+/+} corneas treated with WFA having much higher expression of p21^{Cip1} compared to p27^{Kip1}. One possible explanation is that p21^{Cip1} becomes targeted for degradation in prometaphase by the anaphase-

promoting complex/cyclosome (APC/C^{cdc20}) (63). Thus, if WFA activity were to cause APC/C downregulation in injured *Vim*^{+/+} corneas this would alleviate negative control over p21^{Cip1} to cause p21^{Cip1} levels to become elevated. In fact, WFA has been demonstrated to cause APC/C downregulation and promote G2/M cell cycle arrest (64), which would suggest that this mechanism could be relevant to WFA's activity in the cornea. Given the complexity of regulatory control of Skp2 and APC/C in exacting timed destruction of CKIs, recognition that TGF- β -induced cell cycle arrest occurs by limiting Skp2 expression at post-transcriptional levels via promoting its nuclear translocation and subsequent degradation by APC/C^{cdh1} adds another level of regulation to CKI expression (15, 65). Whether APC/C is also affected by genetic deficiency of vimentin is not known, but may be one possible reason for the basal levels of p21^{Cip1} being higher in *Vim*^{-/-} corneas compared to *Vim*^{+/+} corneas. We postulate that *Vim*^{-/-} corneas having reduced levels of TGF- β may alter the effectiveness of APC/C^{cdh1} to regulate Skp2, and hence, lose control over its nuclear targets in *Vim*^{-/-} corneas. Furthermore, our data suggests that while the mechanism(s) governing induction of Skp2 expression with injury are apparently not affected in vimentin deficiency, a vimentin-independent pathway induced by WFA contributes to partial Skp2 downregulation in injured *Vim*^{-/-} corneas. We speculate that desmin targeting by WFA may be responsible for downregulation of Skp2 expression in *Vim*^{-/-} corneas. Thus, the differential regulation of CKIs in vimentin deficiency remains to be further investigated.

It has recently become recognized that Skp2 acts as a node governing the integration of signals from mechanical tension and growth factors to regulate cell proliferation (66). Such tension-related integration of signaling through Skp2 can impact fibrosis, which was demonstrated by therapeutic delivery of Skp2-targeting siRNAs to provide protection against fibrosis and reduce scarring in a glaucoma filtration surgery model (67). Also, Skp2-deficient mice are protected from renal fibrosis from p27^{Kip1} upregulation in epithelial cells (68). However, in the cornea, desmin is not expressed after simple incision injuries that normally heal without induction of fibrosis (69). This may explain the clinical success of numerous types of scar-less surgical procedures being performed to correct for visual defects of the human cornea (70). However, expression of both vimentin

and desmin are remarkably elevated in corneas that develop opacity, which was illustrated in an animal model of laser photo ablation that emulates the clinical outcomes of failure to heal in this popular type of laser vision corrective procedure (22). Hence, our finding of overproduced desmin in *Vim*^{+/+} fibrotic corneas and persistence of its expression, although at significantly lower levels in *Vim*^{-/-} corneas that display residual opacity or “corneal haze”, was compelling evidence to also investigate desmin as a potential corneal fibrotic mediator. We believe that increased cell stiffness produced by desmin IFs (71) could contribute to altering the viscoelasticity of the cornea (70). In this respect, thermal burn injury increases the stiffness of corneal tissue (72), suggesting that such fibrotic injuries that affect corneal viscoelasticity from edema and increasing intraocular pressure (73) may also be governed by type III IFs. Furthermore, our finding of desmin localization in injured *Vim*^{+/+} corneas at the subepithelial and anterior stroma suggest that the anterior region of alkali-injured *Vim*^{+/+} corneas is also under greater stress than elsewhere. It is intriguing that the anterior region of the cornea is also known to be stiffer than the posterior stroma (74). While the role of desmin in viscoelastic properties of the corneas has not been investigated before, stress studies conducted in other viscoelastic tissues have identified that microarteries (resistant arteries) that express the greatest amounts of desmin were most affected, whereas, large compliance arteries that have low levels of desmin were not when desmin is deficient (75). These resistant arteries are most affected because of their dependence on IFs for maintaining viscoelasticity, where desmin promotes transmission of contractile force to cell surface. Similar studies made in bladder confirm such a role for desmin in viscoelasticity (76). Thus, it remains to be investigated whether the viscoelastic function of desmin is truly responsible for the corneal haze we observed in injured *Vim*^{-/-} corneas.

On the other hand, the reduction of TGF- β , a profibrogenic stimulus for myofibroblast differentiation, in *Vim*^{-/-} mice and in WFA-treated *Vim*^{+/+} mice points to a suppression of a fibrotic switch elicited in genetic and pharmacological deficiency of vimentin. That direct blockade of TGF- β (39) or antagonizing its signaling mechanism in corneal cells (77) inhibits α -SMA expression in corneal stroma and restores corneal clarity in alkali injured mice further supports the idea that this

cytokine is relevant to therapeutic strategies being considered for treatment of corneal fibrotic disorders (37). In this respect, the regulatory control of TGF- β biogenesis and its activity is associated with mechanical forces exerted by stromal myofibroblasts on the extracellular matrix that facilitates a positive feed back loop where mechanical tension in the stroma promotes and sustains the myofibroblast phenotype through activation of α -SMA expression (78). Overexpression of both vimentin and desmin in wound fibroblasts would provide this contractile force and also enable long-distance communication within the mesenchyme of the repairing tissue enabled by polymeric IFs. Through such mechanical tension (79), myofibroblasts/fibroblasts can continuously sense the changing geometry of the corneal stroma as it remodels its injured tissues (80, 36). Indeed, vimentin expression is observed extended to the tips of the fibroblastic cellular processes where these extensions connect over a hundred micrometers in length across the cornea; injured *Vim*^{-/-} corneas would have significant deficits in this tension-induced fibrotic positive feed-back loop, which probably reflects the lower expression levels of α -SMA and TGF- β expression (81) and delayed expression of desmin. Moreover, suggesting a common function of these IFs in cell stiffness that contributes to pathology, increased expression of vimentin and GFAP in retinal glia contributes to glial scarring (82). In a similar vein, overexpression of vimentin with desmin may also contribute to corneal scarring due to increased stiffness of fibroblasts/myofibroblasts because cells that lack vimentin are known to lose their stiffness (19), which may be due to loss of IF-related nanomechanical functions (6).

Lastly, although vimentin and desmin are expressed in the fibrotic cornea, their respective roles are likely to be different. First, desmin expression is rarely observed in α -SMA-expressing myofibroblasts (data not shown). Second, desmin's expression in injured *Vim*^{-/-} corneas occurs at later stages of injury repair when other fibrotic biomarkers were attenuated; this disassociates a role for desmin in fibrotic cell proliferation. Furthermore, overexpressed vimentin but not desmin is observed with corneal opacity in other corneal alkali burn injury models in rabbits (69). While the reason for desmin not upregulated in rabbits is unclear presently, despite this, the critical role of vimentin overexpression in fibrosis is highlighted. On the other hand, our

findings identifying TKT downregulation in fibrotic corneas and its restoration by both genetic absence and pharmacological downregulation of vimentin validates TKT loss as a biomarker of corneal fibrosis (38). This identifies also that TKT regulation in corneal fibrosis may be uncoupled from desmin-related refractive aberrations. In this respect, our findings would support the model that TKT loss contributes significantly to increased refractive properties of myofibroblasts (83), suggesting that TKT-independent mechanisms unveiled in *Vim*^{-/-} corneas may also contribute further to the quality of corneal repair.

In conclusion, our finding that alkali injured *Vim*^{-/-} corneas engage a reparative healing process leading to significant improvement in corneal refractive function came as a surprise because of reports of defective wound repair in *Vim*^{-/-} mice (19, 20). Moreover, vimentin deficiency has also been shown to reduce epithelial cell migration (84). Importantly, these prior studies have investigated the role of vimentin in normal physiological tissue repair, where contribution of vimentin's contractile forces to promote stromal tissue contraction is important to seal a wound with scar tissue (20, 70), while in the epithelium, cell migration is a requirement for resurfacing scrape injuries (84). As embryonic tissue repair is also defective in *Vim*^{-/-} mice (20), which is a situation where myofibroblasts are not involved (85), clearly it is the contextual nature of injury when lack of vimentin expression can be either beneficial or detrimental to the outcome. In this corneal alkali injury model, stromal fibroblast/myofibroblast invasion into the corneal epithelium was also

attenuated by pharmacological and genetic deficiency of vimentin. Thus, from a clinical treatment paradigm traumatic corneal conditions that progress to fibrosis with IF overexpression would most likely benefit from downregulation of vimentin and desmin. Our rationale appears to be consistent also with other traumatic injury models studied in the CNS where the deficiencies of type III IFs have promoted regenerative healing (11). On the other hand, WFA does not show toxicity to sensitive neuroretinal tissues or cause lens cataracts (26, 27), and importantly, *Vim*^{-/-} mice also do not develop cataracts developmentally or have an increased sensitivity to cataracts after being subjected to alkali injury (our unpublished observations). Thus, the recent finding of a vimentin mutation (E151K) in humans, which recapitulates the phenotype of the corresponding genetically engineered mutation in mouse vimentin, causing posterior lens cataracts defines a novel dominant function of mutant vimentin that is cataract specific (86). As no other organ defect has been reported in this human patient or the corresponding mouse model, it is clear that type III IF-genetic mutations cause highly specific organ and tissue-specific disorders (87). The use of WFA to target these type III IFs diseases in mouse models could afford new insight to the treatment of this class of rare human genetic diseases. Taken together, the successful use of WFA to control angiogenesis (16), gliosis (26) and tumor growth and metastasis (28, 88, 89), underscores the broad therapeutic efficacy of this novel type III IF-targeting drug-like molecule and its potential for drug development.

REFERENCES

- Whitcher, J. P., Srinivasan, M., and Upadhyay, M. P. (2001) *Bull. World Health Organ.* **79**, 214-21
- Salomao, M. Q., and Wilson, S. E. (2009) *J. Refract. Surg.* **25**, 459-66
- Taneri, S., Weisberg, M., and Azar, D. T. (2011) *J. Cataract Refract. Surg.* **37**, 392-408
- Qazi, Y., Wong, G., Monson, B., Stringham, J., and Ambati, B. K. (2010) *Brain Res. Bull.* **81**, 198-210
- Schaffeld, M., Herrmann, H., Schultess, J., and Markl, J. (2001) *Eur. J. Cell. Biol.* **80**, 692-702
- Herrmann, H., Bar, H., Kreplak, L., Strelkov, S. V., and Aebi, U. (2007) *Nat. Rev. Mol. Cell. Biol.* **8**, 562-73
- Goldman, R.D., Grin, B., Mendez, M.G., and Kuczumski, E.R. (2008) *Curr. Opin. Cell Biol.* **20**, 28-34
- Helfand, B. T., Chang, L., and Goldman, R. D. (2004) *J. Cell Sci.* **117**, 133-41
- Colucci-Guyon, E., Portier, M.M., Dunia, I., Paulin, D., Pournin, S., and Babinet, C. (1994) *Cell* **79**, 679-94
- Pekny, M. (2001) *Prog. Brain Res.* **132**, 23-30
- Pekny, M., and Pekna, M. (2004) *J. Pathol.* **204**, 428-37
- Lundkvist, A., Reichenbach, A., Betsholtz, C., Carmeliet, P., Wolburg, H., and Pekny, M. (2004) *J. Cell Sci.* **117**, 3481-8
- Pekny, M., Johansson, C. B., Eliasson, C., Stakeberg, J., Wallen, A., Perlmann, T., Lendahl, U., Betsholtz,

- C., Berthold, C. H., and Frisen, J. (1999) *J. Cell Biol.* **145**, 503-14
14. Plodinec, M., Loparic, M., Suetterlin, R., Herrmann, H., Aebi, U., and Schoenenberger, C.A. (2011) *J. Struct. Biol.* **174**, 476-84
 15. Che, X., Chi, F., Wang, L., Jong, T. D., Wu, C.H., Wang, X., and Huang, S. H. (2011) *Brain Pathol.* **21**, 389-404
 16. Bargagna-Mohan, P., Hamza, A., Kim, Y.E., Khuan, Abby Ho Y., Mor-Vaknin, N., Wendschlag, N., Liu, J., Evans, R. M., Markovitz, D. M., Zhan, C. G., Kim, K. B., and Mohan, R. (2007) *Chem. Biol.* **14**, 623-34
 17. Satelli, A., and Li, S. (June 3, 2011) *Cell. Mol. Life Sci.* [Epub ahead of print]
 18. Verardo, M.R., Lewis, G.P., Takeda, M., Linberg, K. A., Byun, J., Luna, G., Wilhelmsson, U., Pekny, M., Chen, D. F., and Fisher, S. K. (2008) *Invest. Ophthalmol. Vis. Sci.* **49**, 3659-65
 19. Eckes, B., Dogic, D., Colucci-Guyon, E., Wang, N., Maniotis, A., Ingber, D., Merckling, A., Langa, F., Aumailley, M., Delouvee, A., Koteliensky, V., Babinet, C., and Krieg, T. (1998) *J. Cell Sci.* **111**, 1897-907
 20. Eckes, B., Colucci-Guyon, E., Smola, H., Nodder, S., Babinet, C., Krieg, T., and Martin, P. (2000) *J. Cell Sci.* **113**, 2455-62
 21. Nieminen, M., Henttinen, T., Merinen, M., Marttila-Ichihara, F., Eriksson, J. E., and Jalkanen, S. (2006) *Nat. Cell Biol.* **8**, 156-62
 22. Chaurasia, S. S., Kaur, H., de Medeiros, F. W., Smith, S. D., and Wilson, S.E. (2009) *Exp. Eye Res.* **89**, 133-9
 23. Ishizaki, M., Zhu, G., Haseba, T., Shafer, S.S., and Kao, W.W. (1993) *Invest. Ophthalmol. Vis. Sci.* **34**, 3320-8
 24. Mohan, R., Hammers, H.J., Bargagna-Mohan, P., Zhan, X. H., Herbstritt, C. J., Ruiz, A., Zhang, L., Hanson, A. D., Conner, B. P., Rougas, J., and Pribluda, V. S. (2004) *Angiogenesis* **7**, 115-22
 25. Mishra, L. C., Singh, B. B., and Dagenais, S. (2000) *Altern. Med. Rev.* **5**, 334-46
 26. Bargagna-Mohan, P., Paranthan, R. R., Hamza, A., Dimova, N., Trucchi, B., Srinivasan, C., Elliott, G. I., Zhan, C. G., Lau, D. L., Zhu, H., Kasahara, K., Inagaki, M., Cambi, F., and Mohan, R. (2010) *J. Biol. Chem.* **285**, 7657-69
 27. Paranthan, R. R., Bargagna-Mohan, P., Lau, D. L., and Mohan, R. (2011) *Mol. Vision* **17**, 1901-8
 28. Lahat, G., Zhu, Q. S., Huang, K. L., Wang, S., Bolshakov, S., Liu, J., Torres, K., Langley, R. R., Lazar, A. J., Hung, M. C., and Lev, D. (2010) *PLoS One* **5**, e10105
 29. Yokota, Y., Bargagna-Mohan, P., Ravindranath, P. P., Kim, K. B., and Mohan, R. 2006. *Bioorg. Med. Chem. Lett.* **16**, 2603-7
 30. Nakayama, K., Nagahama, H., Minamishima, Y. A., Matsumoto, M., Nakamichi, I., Kitagawa, K., Shirane, M., Tsunematsu, R., Tsukiyama, T., Ishida, N., Kitagawa, M., and Hatakeyama, S. (2000) *EMBO J.* **19**, 2069-81
 31. Cook, J. R., Mody, M. K., and Fini M. E. (1999) *Invest. Ophthalmol. Vis. Sci.* **40**, 3122-31
 32. Herrmann, H., Haner, M., Brettel, M., Ku, N.O., and Aebi, U. (1999) *J. Mol. Biol.* **286**, 1403-20
 33. Amano, S., Rohan, R., Kuroki, M., Tolentino, M., and Adamis, A.P. (1998) *Invest. Ophthalmol. Vis. Sci.* **39**, 18-22
 34. Falsey, R. R., Marron, M. T., Gunaherath, G. M., Shirahatti, N., Mahadevan, D., Gunatilaka, A. A., and Whitesell, L. (2006) *Nat. Chem. Biol.* **2**, 33-8
 35. West-Mays, J. A., Cook, J. R., Sadow, P. M., Mullady, D. K., Bargagna-Mohan, P., Strissel, K. J., and Fini, M. E. (1999) *Invest. Ophthalmol. Vis. Sci.* **40**, 887-96
 36. Jester, J. V., Huang, J., Barry-Lane, P.A., Kao, W. W., Petroll, W. M., and Cavanagh, H. D. (1999) *Invest. Ophthalmol. Vis. Sci.* **40**, 1959-67
 37. Tandon, A., Tovey, J. C., Sharma, A., Gupta, R., and Mohan, R. R. 2010. *Curr. Mol. Med.* **10**, 565-78
 38. Stramer, B. M., Cook, J.R., Fini, M. E., Taylor, A., and Obin, M. (2001) *Invest. Ophthalmol. Vis. Sci.* **42**, 1698-706
 39. Saika, S., Miyamoto, T., Yamanaka, O., Kato, T., Ohnishi, Y., Sato, M., Muragaki, Y., Ooshima, A., Nakajima, Y., Kao, W. W., Flanders, K. C., and Roberts, A. B. (2005) *Am. J. Pathol.* **166**, 1393-403
 40. Bargagna-Mohan, P., Ravindranath, P. P., and Mohan, R. (2006) *Invest. Ophthalmol. Vis. Sci.* **47**, 4138-45
 41. Oshima, T., Sonoda, K.H., Tsutsumi-Miyahara, C., Qiao, H., Hisatomi, T., Nakao, S., Hamano, S., Egashira,

- K., Charo, I. F., and Ishibashi, T. (2006) *Br. J. Ophthalmol.* **90**, 218-22
42. Ambati, B. K., Jousseaume, A. M., Kuziel, W. A., Adamis, A. P., and Ambati, J. (2003) *Cornea* **22**, 465-7
43. Nakazawa, T., Takeda, M., Lewis, G. P., Cho, K. S., Jiao, J., Wilhelmsson, U., Fisher, S. K., Pekny, M., Chen, D. F., and Miller, J. W. (2007) *Invest. Ophthalmol. Vis. Sci.* **48**, 2760-8
44. Yoshida, K., Nakayama, K., Nagahama, H., Harada, T., Harada C, Imaki, J., Matsuda, A., Yamamoto, K., Ito, M., and Ohno, S. (2002) *Invest. Ophthalmol. Vis. Sci.* **43**, 364-70
45. Zieske, J. D. (2000) *Prog. Retin. Eye Res.* **19**, 257-70
46. Kase, S., Yoshida, K., Ohgami, K., Shiratori, K., Ohno, S., and Nakayama, K. I. (2006) *Curr. Eye Res.* **31**, 307-12
47. Nakayama, K., Nagahama, H., Minamishima, Y. A., Miyake, S., Ishida N, Hatakeyama, S., Kitagawa, M., Iemura, S., Natsume, T., and Nakayama, K. I. (2004) *Dev. Cell* **6**, 661-72
48. Herrmann, H., and Aebi, U. (2004) *Annu. Rev. Biochem.* **73**, 749-89
49. Mackey, D. A., Wilkinson, C. H., Kearns, L. S., and Hewitt, A. W. (2011) *Clin. Experiment. Ophthalmol.* **39**, 462-71
50. Conway, B. R., Chatterjee, S., Field, G. D., Horwitz, G. D., Johnson, E. N., Koida, K., and Mancuso, K. (2010) *J. Neurosci.* **30**, 14955-63
51. Dyer, M. A., and Cepko, C. L. (2000) *Nat. Neurosci.* **3**, 873-80
52. Vij, N., Roberts, L., Joyce, S., and Chakravarti, S. (2004) *Exp. Eye Res.* **78**, 957-71
53. Yoon, M., Moir, R. D., Prahlad, V., and Goldman, R. D. (1998) *J. Cell Biol.* **143**, 147-57
54. Soellner, P., Quinlan, R. A., and Franke, W. W. (1985) *Proc. Natl. Acad. Sci. U.S.A* **82**, 7929-33
55. Chou, Y. H., Flitney, F. W., Chang, L., Mendez, M., Grin, B., and Goldman, R. D. (2007) *Exp. Cell Res.* **313**, 2236-43
56. Moon, R. T., and Lazarides, E. (1983) *Proc. Natl. Acad. Sci. U.S.A* **80**, 5495-9
57. Skalli, O., Chou, Y. H., and Goldman, R. D. (1992) *Proc. Natl. Acad. Sci. U.S.A* **89**, 11959-63
58. Franke, W. W., Schmid, E., Grund, C., and Geiger, B. (1982) *Cell* **30**, 103-13
59. Chang, H. C., Chang, F. R., Wang, Y. C., Pan, M. R., Hung, W. C., and Wu, Y. C. (2007) *Mol. Cancer Ther.* **6**, 1572-8
60. Hara, T., Kamura, T., Nakayama, K., Oshikawa, K., Hatakeyama, S. (2001) *J. Biol. Chem.* **276**, 48937-43
61. Bornstein, G., Bloom, J., Sitry-Shevah, D., Nakayama, K., Pagano, M., and Hershko, A. (2003) *J. Biol. Chem.* **278**, 25752-7
62. Bond, M., and Wu, Y. J. (2011) *Front. Biosci.* **16**, 1517-35
63. Amador, V., Ge, S., Santamaria, P. G., Guardavaccaro, D., and Pagano, M. (2007) *Mol. Cell* **27**, 462-73
64. Stan, S. D., Zeng, Y., and Singh, S. V. (2008) *Nutr. Cancer* **60** Suppl 1, 51-60
65. Hu, D., Liu, W., Wu, G., and Wan, Y. (2011) *Cell Cycle* **10**, 285-92
66. Jiang, X., Austin, P. F., Niederhoff, R. A., Manson, S. R., Riehm, J. J., Cook, B. L., Pengue, G., Chitaley, K., Nakayama, K., Nakayama, K. I., and Weintraub, S. J. (2009) *Mol. Cell Biol.* **29**, 5104-14
67. Wang, F., Qi, L.X., Su, Y., Yan, Q. H., and Teng, Y. (2010) *Invest. Ophthalmol. Vis. Sci.* **51**, 1475-82
68. Suzuki, S., Fukasawa, H., Kitagawa, K., Uchida, C., Hattori, T., Isobe, T., Oda, T., Misaki, T. Ohashi, N., Nakayama, K., Nakayama, K. I., Hishida, A., Yamamoto, T., and Kitagawa, M. (2007) *Am. J. Pathol.* **171**, 473-83
69. Ishizaki, M., Wakamatsu, K., Matsunami, T., Yamanaka, N., Saiga, T., Shimizu, Y., Zhu, G., and Kao, W. W. (1994) *Exp. Eye Res.* **59**, 537-49
70. Dupps, W. J., Jr., and Wilson, S. E. (2006) *Exp. Eye Res.* **83**, 709-20
71. Schopferer, M., Bar, H., Hochstein, B., Sharma, S., Mucke, N., Herrmann, H., and Willenbacher, N. (2009) *J. Mol. Biol.* **388**, 133-43
72. Tanter, M., Touboul, D., Gennisson, J. L., Bercoff, J., and Fink, M. (2009) *IEEE Trans. Med. Imaging* **28**, 1881-93
73. Macsai, M. S. (2000) *Cornea* **19**, 617-24
74. Muller, L. J., Pels, E., and Vrensen, G. F. (2001) *Br. J. Ophthalmol.* **85**, 437-43
75. Lacolley, P., Challande, P., Boumaza, S., Cohuet, G., Laurent, S., Boutouyrie, P., Grimaud, J. A., Paulin, D., Lamaziere, J. M., and Li, Z. (2001) *Cardiovasc. Res.* **51**, 178-87

76. Scott, R. S., Li, Z., Paulin, D., Uvelius, B., Small, J. V., and Arner, A. (2008) *Am. J. Physiol. Cell. Physiol.* **295**, C324-31
77. Saika, S., Ikeda, K., Yamanaka, O., Flanders, K. C., Nakajima, Y., Miyamoto, T., Ohnishi, Y., Kao, W. W., Muragaki, Y., and Ooshima, A. (2005) *Lab Invest.* **85**, 474-86
78. Tomasek, J. J., Gabbiani, G., Hinz, B., Chaponnier, C., and Brown, R. A. (2002) *Nat. Rev. Mol. Cell. Biol.* **3**, 349-63
79. Petroll, W., Vishwanath, M., and Ma, L. (2004) *Invest. Ophthalmol. Vis. Sci.* **45**, 3466-74
80. Hassell, J. R., and Birk, D. E. (2010) *Exp. Eye Res.* **91**, 326-35
81. Zhao, X. H., Laschinger, C., Arora, P., Szaszi, K., Kapus, A., McCulloch, C. A. (2007) *J. Cell Sci.* **120**, 1801-9
82. Lu, Y. B., Iandiev, I., Hollborn, M., Korber, N., Ulbricht, E., Hirrlinger, P. G., Pannicke, T., Wei, E. Q., Bringmann, A., Wolburg, H., Wilhelmsson, U., Pekny, M., Wiedemann, P., Reichenbach, A., and Kas, J. A. (2011) *Faseb J.* **25**, 624-31
83. Jester, J. V., Petroll, W. M., and Cavanagh, H. D. (1999) *Prog. Retin. Eye Res.* **18**, 311-56
84. Rogel, M. R., Soni, P. N., Troken, J. R., Sitikov, A., Trejo, H. E., and Ridge, K. M. (June 29, 2011) *Faseb J.* [Epub ahead of print]
85. Hopkinson-Woolley, J., Hughes, D., Gordon, S., Martin, P. (1994) *J. Cell Sci.* **107**, 1159-67
86. Muller, M., Bhattacharya, S.S., Moore, T., Prescott, Q., Wedig, T., Herrmann, H., and Magin, T. M. (2009) *Hum. Mol. Genet.* **18**, 1052-7
87. Bar, H., Mucke, N., Ringler, P., Muller, S. A., Kreplak, L., Katus, H. A, Aebi, U., and Herrmann, H. (2006) *J. Mol. Biol.* **360**, 1031-42
88. Thaiparambil, J. T., Bender, L., Ganesh, T., Kline, E., Patel, P., Liu, Y., Tighiouart, M., Vertino, P. M., Harvey, R. D., Garcia, A., and Marcus, A. I. (Jan 20, 2011) *Int. J. Cancer* 10.1002/ijc.25938
89. Maxwell, S. A., Cherry, E. M., and Bayless, K. J. (2011) *Leuk. Lymphoma* **52**, 849-64

Acknowledgements- This work was supported in part by the John A. and Florence Mattern Solomon Endowed Chair in vision biology and eye diseases to R.M. and funds from his R01 EY0167821, R01 CA131059, Fight for Sight, Inc., and KSEF-578-RDE-005 (Kentucky Science and Engineering Foundation) grants. Authors also thank NIH grant support from R01 DA013930, R01 DA025100, and R01 DA021416 (C.-G.Z.). Thanks also to J. Ambati, M. Fannon and A. Pearson for many useful scientific discussions. We also thank S. Crocker, C. Shaw and A. Thomson for help with image scoring. We thank Jack Goodman (UK mass spectrometry core center), Mary Gail Engle (UK imaging facility), Maya Yankova (UCHC electron microscopy facility), Glenn Florence (UK animal housing facilities) and Greg Bauman (UK flow cytometry core center) for their technical assistance.

FOOTNOTES

²The abbreviations used are: LASIK, laser in situ keratomileusis; WFA, withaferin A; WFA-Bt, withaferin A-biotin; IF, intermediate filament; CNS, central nervous system; *Vim*^{-/-} -vimentin-deficient; TGF- β , transforming growth factor- β ; TBS, Tris-buffered saline; TBST, Tris-buffered saline with Tween-20; SDS, sodium dodecylsulfate; DMSO, dimethyl sulfoxide; PBS, phosphate buffered saline; PMSF, phenylmethylsulfonyl fluoride; MD, molecular dynamics; ULF, unit length filament; GAPDH, glyceraldehyde phosphate dehydrogenase; α -SMA, α -smooth muscle actin; LC-MS, liquid chromatography-mass spectrometry; LC-ESI-MS-MS, liquid chromatography-electron spray ionization tandem mass spectrometry; TKT, transketolase; MEFs, mouse embryonic fibroblasts; CKI, cyclin dependent kinase inhibitor; GFAP, glial fibrillary acidic protein; Skp2, S-phase kinase-associated protein-2; DAPI, 4,6-diamidino-2-phenylindole; MEM, minimal essential medium; PMN, polymorphonuclear neutrophil.

FIGURE LEGENDS

FIGURE 1. Control of vimentin expression favors corneal clarity in the alkaline burn injury model. *Vim*^{+/+} and *Vim*^{-/-} mice were subjected to corneal chemical injury with limbal and corneal epithelial cell debridement and treated daily with DMSO (Veh) or 2 mg/kg/d of WFA by intraperitoneal injection for 7 and 14 days. (A) Representative images at d14 of *Vim*^{+/+} and *Vim*^{-/-} whole eyes show dramatic reduction of corneal opacity in mice that have vimentin expression down-regulated either pharmacologically (WFA) or genetically (*Vim*^{-/-}). (B) Quantification of corneal opacity by biomicroscopy at d14 using an opacity scale 0 (clear) to 4 (opaque) (n = 8 samples/group). (C) Vimentin expression is down regulated pharmacologically by WFA at d7 as shown by western blot analysis of corneal buttons from uninjured (Unj), injured vehicle-treated (Veh) and WFA-treated *Vim*^{+/+} mice. Blots were probed sequentially with antibodies against vimentin (clone V9), annexin II and β -actin was used as loading control. Data is representative of two independent experiments (n= 4 mice/group). (D) Densitometric quantification of vimentin and annexin II normalized to β -actin using ImageJ software. (E) Immunofluorescence staining of vimentin expression (green) in thin tissue sections from corneas of Unj, Veh and WFA-treated *Vim*^{+/+} mice at d7 and d14. Image of Unj sample is enhanced compared to Veh and WFA samples to reveal low level of vimentin staining in corneal stromal keratocytes (white arrows). Nuclei are stained with 4',6-diamidino-2-phenylindole (DAPI, blue). Bars, 150 μ m. Data are representative of two independent experiments (n= 4 mice/group). (F) Affinity isolation of WFA-bt binding proteins from rabbit corneal fibroblasts. Corneal keratocytes were differentiated *in vitro* to wound fibroblasts and pre-incubated with DMSO (vehicle) or with 5 μ M WFA for 30 min and subsequently both treatment groups were incubated with 5 μ M WFA-bt for 2 hr. Soluble protein lysates (SL) were obtained and subsequently purified over NeutrAvidin affinity columns and western blotted by probing for vimentin and annexin II. A small amount of soluble lysate was included in parallel to demonstrate presence of vimentin and annexin II in corneal cells. Error bars represent the SD.

FIGURE 2. Corneal fibrosis is mediated by vimentin. *Vim*^{+/+} and *Vim*^{-/-} mice were subjected to corneal alkali injury and treated daily with vehicle (Veh) or 2 mg/kg/d WFA by intraperitoneal injection for 7 and 14 days. (A and B) Immunofluorescence staining of α -SMA (red) in repairing corneas of *Vim*^{+/+} (A) and *Vim*^{-/-} (B) mice treated with vehicle or WFA. Nuclei were stained with DAPI (blue). Epi = epithelium; St = stroma. Bar, 150 μ m. Data are representative of two independent experiments (n = 8/group). (C) Immunoblot analysis of α -SMA expression in corneal tissues from Unj and injured *Vim*^{+/+} and *Vim*^{-/-} mice at d7 and d14 treated with Veh or WFA and GAPDH was used as loading control. (D) Densitometric quantification of α -SMA expression normalized to GAPDH. Error bars represent the SD.

FIGURE 3. WFA downregulates TGF- β expression in injured corneas. (A) *Vim*^{+/+} and *Vim*^{-/-} mice were subjected to corneal alkali injury and treated daily with Veh or 2 mg/kg/d WFA by intraperitoneal injection for 14 days. Immunofluorescence staining of TGF- β 2 (green) in Unj and injured corneas of *Vim*^{+/+} and *Vim*^{-/-} mice. Nuclei were stained with DAPI (blue). Data are representative of two independent experiments (n = 8/group). (B) Differentiation of *Vim*^{+/+} and *Vim*^{-/-} fibroblasts to myofibroblasts with TGF- β treatment in presence and absence of 500 nM WFA. Expression of α -SMA expression (red) was assessed by immunofluorescence staining and counterstained with DAPI to mark nuclei (blue). (C) Percent of cells expressing α -SMA to total number of cell nuclei from three replicates. Data are representative of two independent experiments (n= 9/group). (D) Western blot analysis of corneal tissues from Unj and injured d14 *Vim*^{+/+} and *Vim*^{-/-} mice treated with vehicle or WFA. Blots were probed with polyclonal antibody to TKT followed by β -actin. (E) Densitometric quantification of TKT normalized to β -actin using ImageJ. (F) Transmission electron microscopy (TEM) of mouse corneas. *Vim*^{+/+} and *Vim*^{-/-} mice were subjected to corneal alkali injury and treated daily with Veh or 2 mg/kg/d WFA for 14 days. TEM images of corneas from Veh-treated *Vim*^{+/+} mice reveal well-differentiated myofibroblasts having an abundance of rough endoplasmic reticuli (a, arrow). The epithelial basement membrane appears to be intact (a, arrowheads). The presence of PMNs is also observed in Veh samples (b, arrow). In comparison, corneas of uninjured *Vim*^{+/+} mice reveal typical staining pattern for keratocytes (c,

arrow). Corneas of *Vim*^{+/+} injured mice treated with WFA reveal mostly keratocytes and wound fibroblasts (d, arrow) and myofibroblasts (not shown) were only rarely found. Injured *Vim*^{-/-} corneas also contain keratocytes/fibroblasts, which was similarly observed in injured corneas of *Vim*^{-/-} mice treated with WFA (d and e, arrows). Error bars represent the SD.

FIGURE 4. WFA downregulates expression of inflammatory markers during corneal repair. *Vim*^{+/+} and *Vim*^{-/-} mice were subjected to corneal alkali injury and treated daily with Veh or 2 mg/kg/d of WFA for 7 and 14 days. (A) Immunoblot analysis of corneal tissues from Unj and injured *Vim*^{+/+} and *Vim*^{-/-} mice at d7 treated with Veh or WFA. (B) Densitometric quantification of IκB-α normalized to β-actin. (C) Immunolocalization of p65 RelA/NF-κB staining (green) in the epithelium of *Vim*^{+/+} and *Vim*^{-/-} corneas at d14 showing nuclear localization of p65 (white arrows in basal layer) in Veh-treated *Vim*^{+/+} sample. Bar, 10 μm. (D) Percentage of cells showing p65/RelA staining in nuclei of epithelial cells was determined by comparing with DAPI-staining (not shown). Data are representative of two independent experiments (n=8/group). (E) Immunofluorescence staining of CD11b (green) in *Vim*^{+/+} and *Vim*^{-/-} corneas at d14. Nuclei were counterstained with DAPI (blue). Epi = epithelium; St = stroma. Bar, 150 μm. Data are representative of two independent experiments (n = 8/group). (F) Numbers of CD11b⁺ cells detected in corneal tissue sections (n = 8/group). * *P* = 0.0025; ** *P* = 0.010; ****P* = 0.0053. Error bars represent the SD.

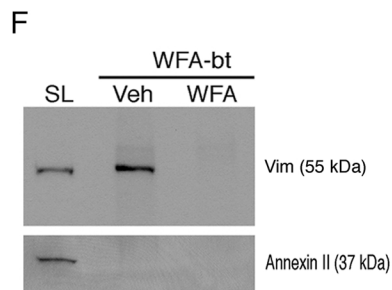
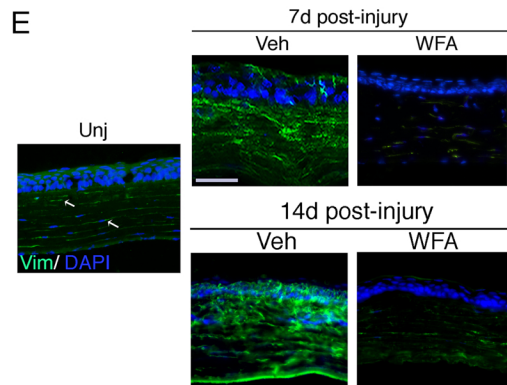
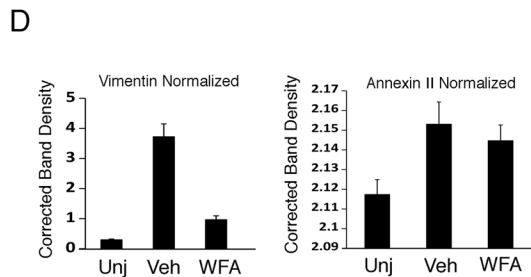
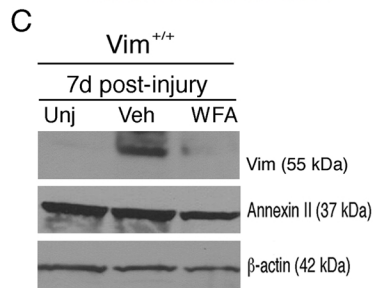
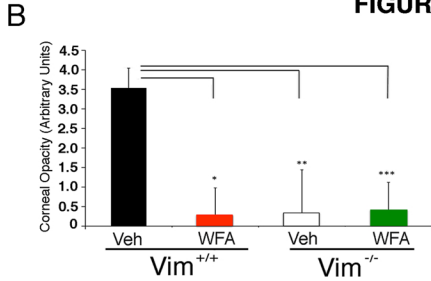
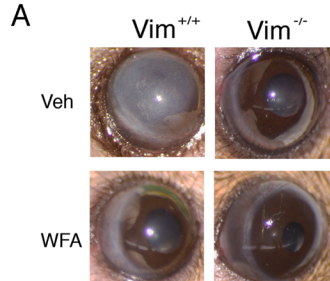
FIGURE 5. WFA's cell cycle activity during corneal repair is mediated by vimentin. *Vim*^{+/+} and *Vim*^{-/-} mice were subjected to corneal alkali injury and treated daily with Veh or 2 mg/kg/d WFA for 7 and 14 days. Corneal tissues were isolated and equal amount of protein extracts were subjected to western blotting and probed sequentially with antibodies against p27^{Kip1}, p21^{Cip1}, and cyclin E (A and C). Blots from d14 samples were also probed with antibody to Skp2. (E) Densitometric quantification of proteins to GAPDH (B and D) and β-actin (F) was performed using NIH ImageJ. (G) Immunolocalization of p27^{Kip1} staining (green) in the epithelium of *Vim*^{+/+} and *Vim*^{-/-} corneas at d7 and d14. Double arrowheads delimit the epithelium in injured (Veh) samples. Data are representative of two independent experiments (n= 8 /group). Bar, 50 μm. (H) WFA induces G₂/M cell cycle arrest. Embryonic fibroblasts from wild-type (WT), p27^{Kip1}^{-/-}, and Skp2-deficient mice were stimulated to proliferate in presence of Veh or WFA and subjected to flow cytometry for cell cycle analysis. Data are representative of two independent experiments. Error bars represent the SD.

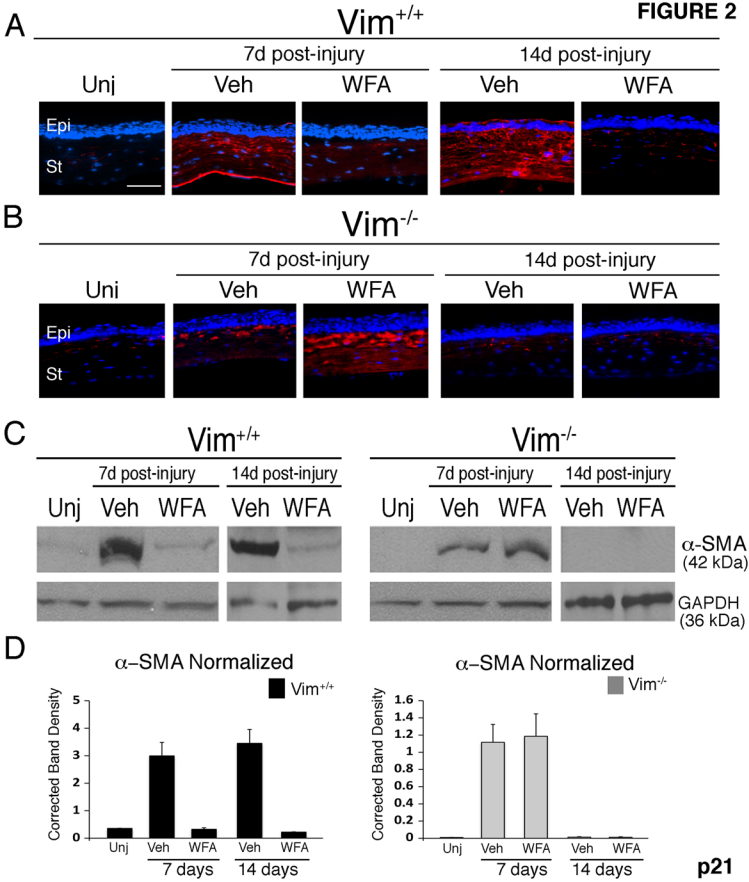
FIGURE 6. Molecular model of WFA-desmin. Atomic model of tetramers formed by head-to-tail dimers in the A₁₁ and A₂₂ configurations (A) that was assembled using a part of a graphic representation previously published (48). (B) Ribbon representation of the MD-simulated desmin-WFA complex structure overlapped with vimentin-WFA complex. (a) Superposition of the desmin-WFA complex with the previously simulated vimentin-WFA complex (16) in which the ribbon structures of the desmin and vimentin are in white and blue, respectively. Amino acids that hydrogen bond with ring A of the ligand are represented by their stick structures (b). Ribbon structure of desmin-WFA showing hydrogen bonds between Q329 and C1-ketone of WFA and D336 with C4-hydroxyl group of WFA. The β-oriented 5-6 epoxide of WFA is positioned for nucleophilic attack by C333 (yellow dotted arrow).

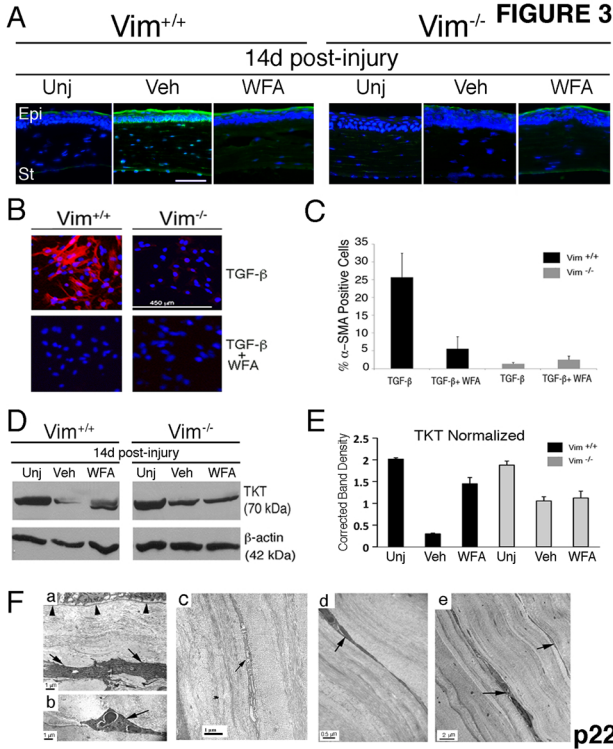
FIGURE 7. WFA downregulates injury-induced desmin expression in healing corneas. *Vim*^{+/+} and *Vim*^{-/-} mice were subjected to corneal alkali injury and treated daily with Veh or 2 mg/kg/d of WFA for 7 and 14 days. (A and B) Temporal induction and localization of desmin (green) in repairing tissues of corneas from *Vim*^{+/+} (A) and *Vim*^{-/-} (B) corneas from Unj, Veh and WFA-treated mice. Higher magnified images of *Vim*^{-/-} corneal sections at d14 reveals a novel dot-like staining pattern for desmin in the epithelium (i) that appears nuclear-associated. Nuclei were stained with DAPI (blue). Epi = epithelium; St = stroma. Bar, 200 μm. Data are representative of two independent experiments (n= 8/group). (C) Total corneal tissue lysates were also prepared from d7 and d14 mice and subjected to western blotting and probed with desmin antibody. Asterisk indicates the major 52-kDa protein species, and arrowhead and arrow indicate lower molecular weight desmin species/variants differentially regulated. (D) Densitometric quantification of desmin in *Vim*^{+/+} and *Vim*^{-/-}

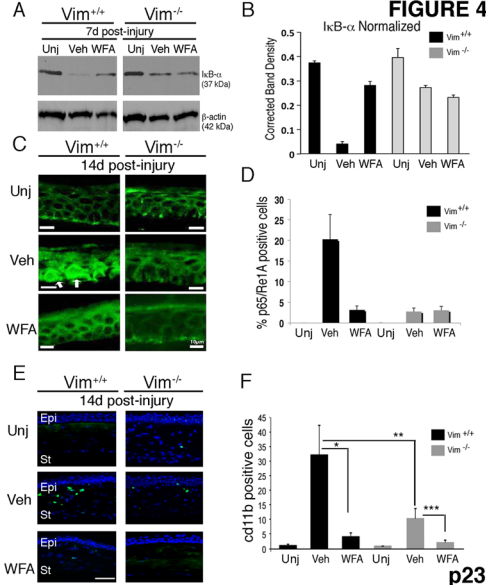
samples normalized to GAPDH. (E) Western blot analysis of soluble desmin from corneas of d14 *Vim*^{+/+} and *Vim*^{-/-} mice. Asterisk indicates the major 52-kDa band and arrowhead and arrow indicate smaller-sized desmin variants; open circle is a non-specific band. (F) Densitometric quantification of soluble desmin in *Vim*^{+/+} and *Vim*^{-/-} samples normalized to GAPDH. Error bars represent the SD.

FIGURE 8. Computer-aided imaging analysis of corneal transparency. (A) Representative images of injured (Veh) and WFA-treated corneas of *Vim*^{+/+} and *Vim*^{-/-} mice showing opacity that ranked at 50th percentile for corneal clarity. (B) Corneal clarity values for *Vim*^{+/+} and *Vim*^{-/-} mice treated with and without WFA (n > 150 images/group) was plotted as a function of their percentile rank distributions to reveal the trends in healing for each group. Maximal clarity scores at 4.0.









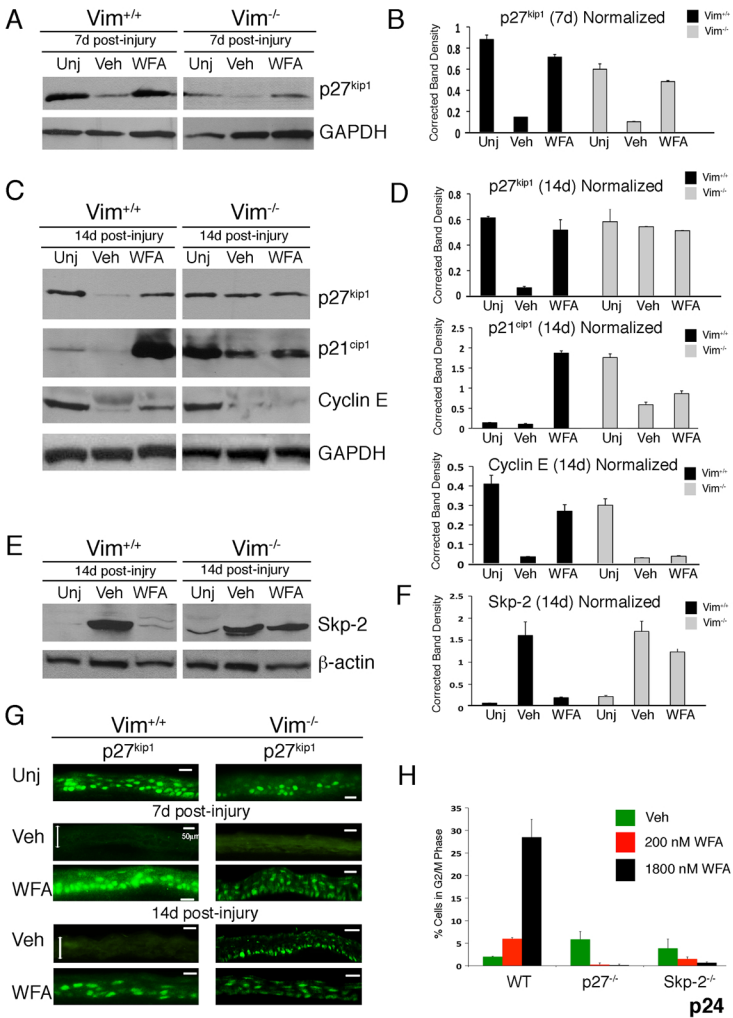
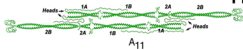
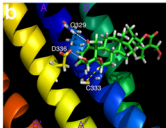
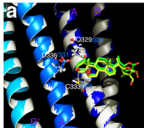
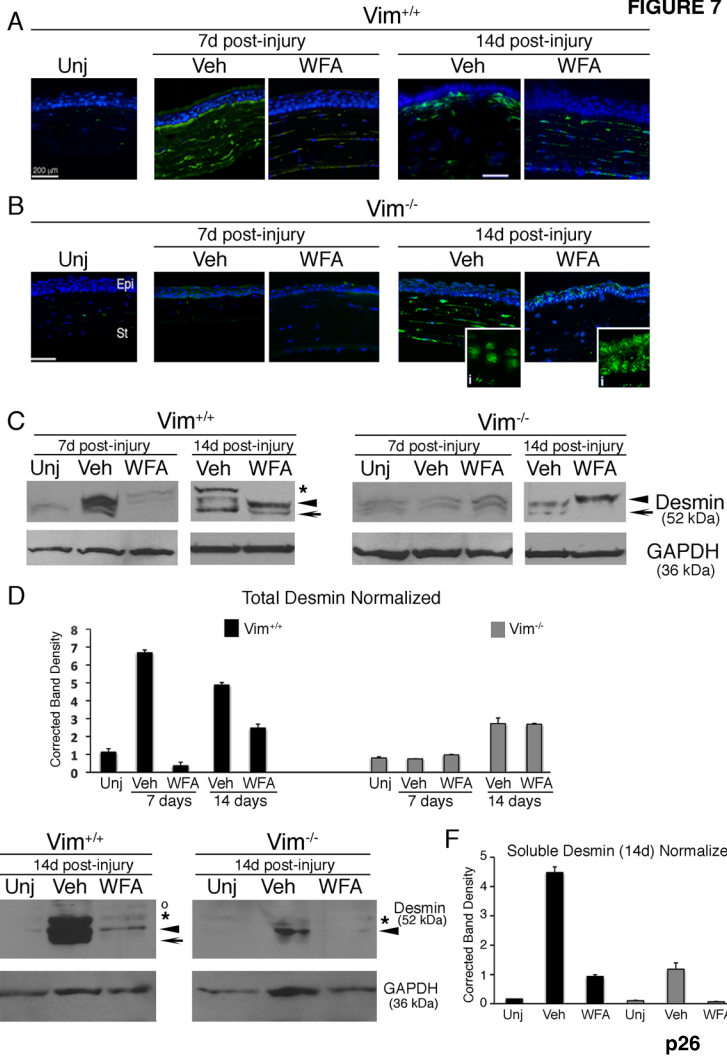
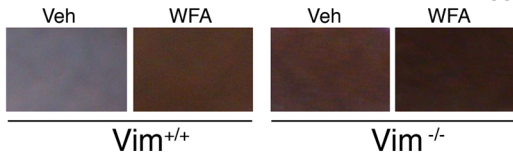


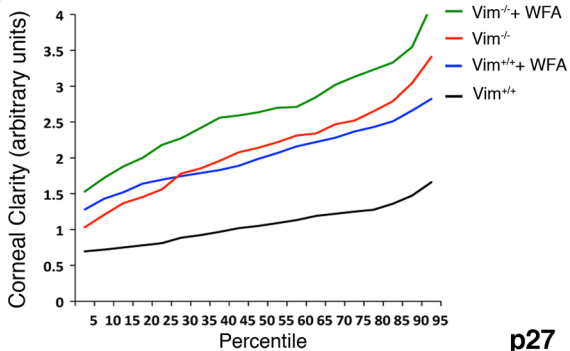
FIGURE 6**A****B**



A



B



p27

SUPPLEMENTAL DATA:

A Corneal Anti-Fibrotic Switch Identified in Genetic and Pharmacological Deficiency of Type III Intermediate Filaments

Paola Bargagna-Mohan¹, Riya R. Paranthan², Adel Hamza³, Chang-Guo Zhan³, Do-Min Lee³, Kyung Bo Kim³, Daniel L. Lau⁴, Cidambi Srinivasan⁵, Keiko Nakayama⁶, Keiichi I. Nakayama⁷, Harald Herrmann⁸, and Royce Mohan^{1*}

From Department of Neuroscience¹, University of Connecticut Health Center, Farmington, CT; Department of Ophthalmology & Visual Sciences², Department of Pharmaceutical Sciences³, Department of Computer and Electrical Engineering⁴, and Department of Statistics⁵, University of Kentucky, Lexington, Kentucky; Division of Developmental Genetics⁶, Tohoku University Graduate School of Medicine, Miyagi, Japan; Department of Molecular and Cellular Biology⁷, Kyushu University, Fukuoka, Japan; and Functional Architecture of the Cell Group, German Cancer Research Center (DKFZ)⁸, Heidelberg, Germany.

Running title: Vimentin is a Fibrosis Target

*Address correspondence to: Royce Mohan, PhD, John A. and Florence Mattern Solomon Endowed Chair in Vision Biology and Eye Diseases, Laboratory of Chemical Biology & Drug Discovery, Department of Neuroscience, University of Connecticut Health, 263 Farmington Ave, Farmington, CT 06030-3401. Tel: 860 679 2020; E-mail: Mohan@UCHC.edu

SUPPLEMENTAL FIGURE LEGENDS

Figure S1. Vimentin-overexpressing stromal fibroblasts invade injured corneal epithelium. $Vim^{+/+}$ mice were subjected to corneal alkali injury and treated daily with vehicle (Veh) or 2 mg/kg/d WFA by intraperitoneal injection for 14 days. (A and B) Immunofluorescence staining of vimentin (green) and E-cadherin (red) in uninjured (Unj) corneas or injured corneas of $Vim^{+/+}$ mice treated with Veh or WFA. Nuclei were stained with DAPI (blue). Bar, 150 μm (A). Image of Unj sample is enhanced compared to Veh and WFA samples to reveal low level of vimentin staining in Unj corneal keratocytes (white arrows). (B) Selected region (white box) from Veh sample has been magnified to show details of filamentous vimentin expression in invasive fibroblasts found in the epithelium. Bar, 10 μm . Data are representative of two independent experiments ($n = 8/\text{group}$).

Figure S2. Transmission Electron Microscopy of alkali injured corneas. $Vim^{+/+}$ and $Vim^{-/-}$ mice were subjected to corneal alkali injury and treated daily with vehicle (Veh) or 2 mg/kg/d WFA for 14 days. TEM images of injured $Vim^{+/+}$ corneas reveal an abundance of conjunctivalized epithelia evidenced by persistence of goblet cells (a, arrow). Elsewhere in the injured corneas of $Vim^{+/+}$ mice basal cells reveal corneal epithelial characteristics (b, arrow) and presence of hemidesmosomes appear intact (b, inset arrows; epi = epithelium, str = stroma). The epithelia of injured corneas from $Vim^{+/+}$ mice treated with WFA appear normal (c, arrow). Corneas of injured $Vim^{-/-}$ mice also were similarly shown to recover from injury and display corneal epithelial characteristics as well as those from $Vim^{-/-}$ mice treated with WFA (d and e, arrows). Epithelial cells from uninjured corneas of $Vim^{+/+}$ mice (f, arrow) and from $Vim^{-/-}$ mice (g, arrow) are shown for comparison. A keratocyte (g, large arrowhead) in corneal stroma of uninjured $Vim^{-/-}$ mice. Small arrowheads in a-e demarcate the overlying epithelium from basement membrane.

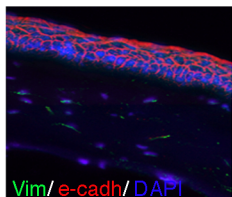
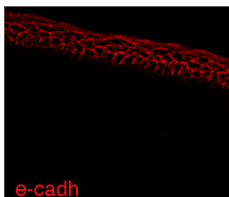
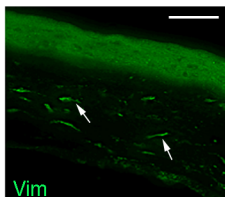
Figure S3. Alignment of desmin and vimentin amino acid fragments used in the molecular modeling studies. The EMBOSS Needle-alignment software from EMBL-EBI was employed to compare the homology between human desmin and vimentin segments from the 2B region contained within the WFA binding site. The cysteine residue (Cys333) that forms a covalent bond with WFA is labeled in red. The amino acids of desmin and vimentin that form hydrogen bonds with WFA are labeled in blue (Gln329) and green (Asp336). The amino acid numbering is for the human desmin polypeptide.

Figure S4. WFA binds soluble recombinant human desmin. Recombinant human tetrameric desmin was incubated for 1 h at 37°C with 5 μM WFA and tryptic digests subjected to analysis by liquid chromatography mass spectrometry. The LC-ESI-MS-MS scans of peptide chromatogram for the tryptic peptides HQIQSYTC'EIDALKGTNDSLMR and HQIQSYTC'EIDALK show an increase by the mass of WFA in the $b7^+$ and $y7^+$ (singly charged fragment ions) and $b7^{2+}$ and $y7^{2+}$ (doubly charged fragment ions) due to the covalent modification of cysteine residue. The ions observed in the analysis are marked in red and blue.

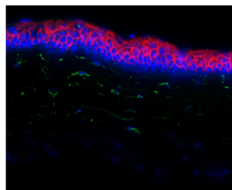
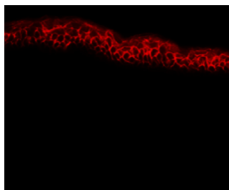
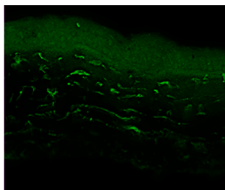
A

14d post-injury

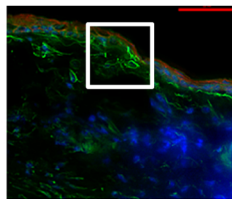
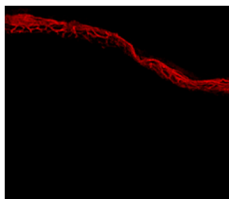
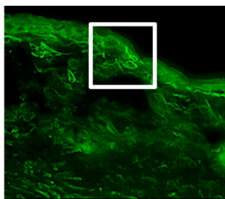
Unj



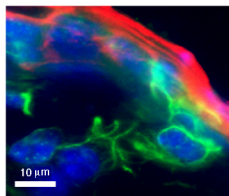
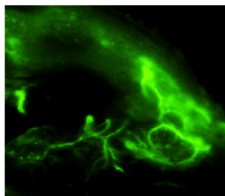
WFA



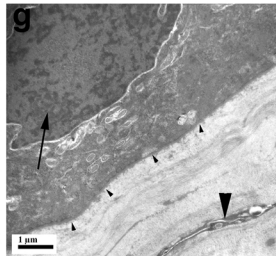
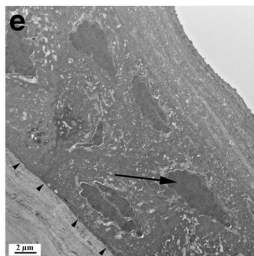
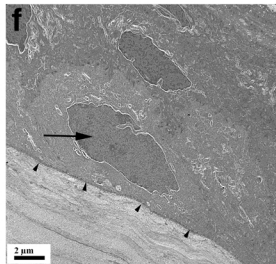
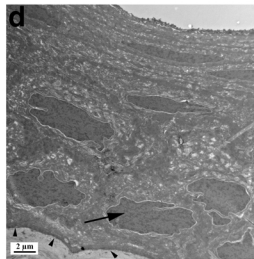
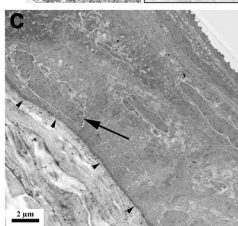
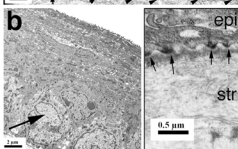
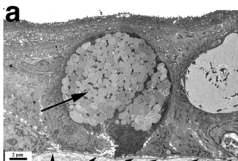
Veh



B



p30



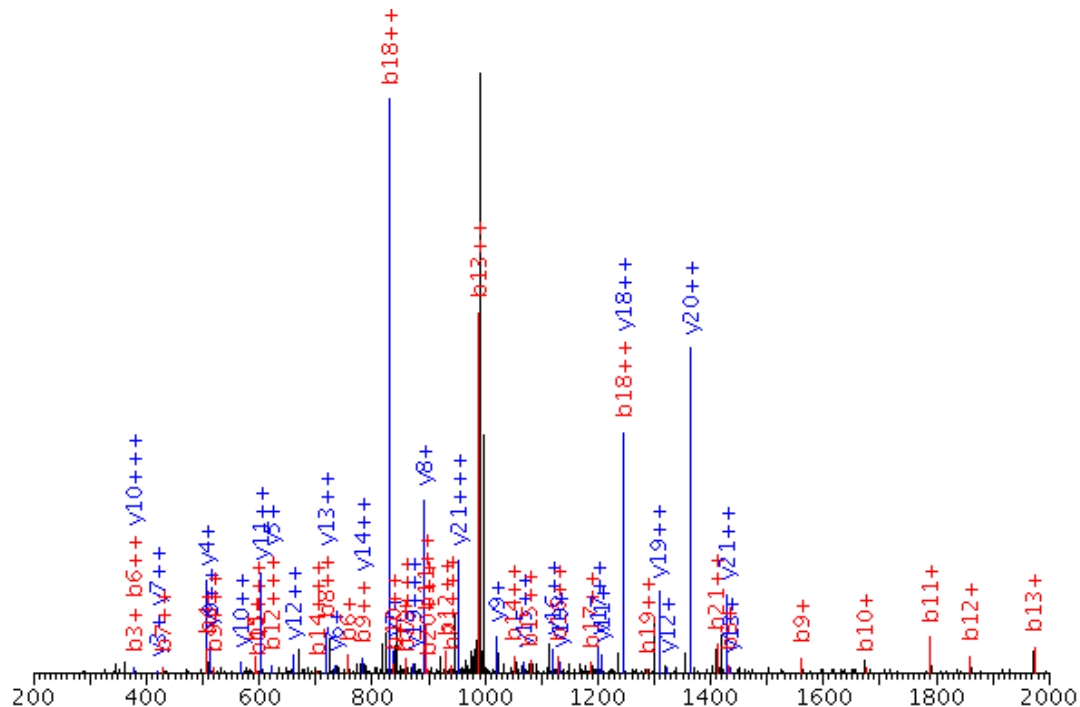
R.HQIQSYTC'EIDALKGTNDSLMR.Q 1284 3+ 85 49.100 10.800 37% 2993.4670 +0.6650 0.9915 9
sp|P17661|DESM_HUMAN

<< Prev

Next >>

Show Modifications

Find Features

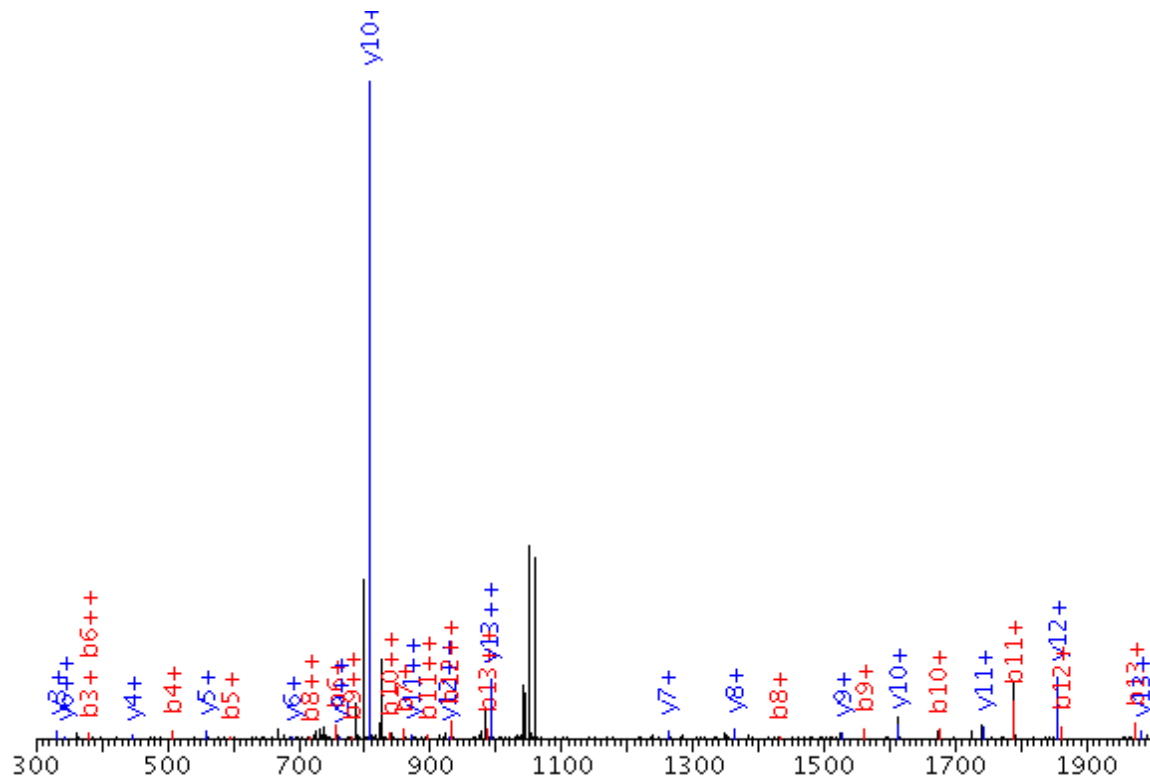


b ³⁺	b ²⁺	b ⁺	#	AA	#	y ⁺	y ²⁺	y ³⁺
46.7216	69.5785	138.1490	1	H	22			
89.4319	133.6438	266.2797	2	Q	21	2857.9551	1429.4815	953.3237
127.1517	190.2236	379.4392	3	I	20	2729.8244	1365.4162	910.6134
169.8619	254.2889	507.5699	4	Q	19	2616.6649	1308.8364	872.8936
198.8880	297.8280	594.6481	5	S	18	2488.5342	1244.7711	830.1834
253.2800	379.4160	757.8241	6	Y	17	2401.4560	1201.2320	801.1573
286.9817	429.9685	858.9291	7	T	16	2238.2800	1119.6440	746.7653
478.1179	716.6729	1432.3379	8	C'	15	2137.1750	1069.0915	713.0636
521.1564	781.2307	1561.4534	9	E	14	1563.7662	782.3871	521.9274
558.8762	837.8104	1674.6128	10	I	13	1434.6507	717.8293	478.8889
597.2391	895.3547	1789.7014	11	D	12	1321.4913	661.2496	441.1690
620.9320	930.8941	1860.7802	12	A	11	1206.4027	603.7053	402.8062
658.6519	987.4738	1973.9397	13	L	10	1135.3239	568.1659	379.1132
701.3765	1051.5609	2102.1138	14	K	9	1022.1644	511.5862	341.1934
720.3939	1080.0868	2159.1657	15	G	8	893.9903	447.4991	298.6687
754.0955	1130.6394	2260.2708	16	T	7	836.9384	418.9732	279.6514
792.1302	1187.6913	2374.3746	17	N	6	735.8333	368.4206	245.9497
830.4930	1245.2356	2489.4632	18	D	5	621.7295	311.3687	207.9151
859.5191	1288.7747	2576.5414	19	S	4	506.6409	253.8244	169.5523
897.2389	1345.3544	2689.7008	20	L	3	419.5627	210.2853	140.5262
940.9698	1410.9507	2820.8934	21	M	2	306.4033	153.7056	102.8064
			22	R	1	175.2107	88.1093	59.0755

R.HQIQSYTC'EIDALK.G

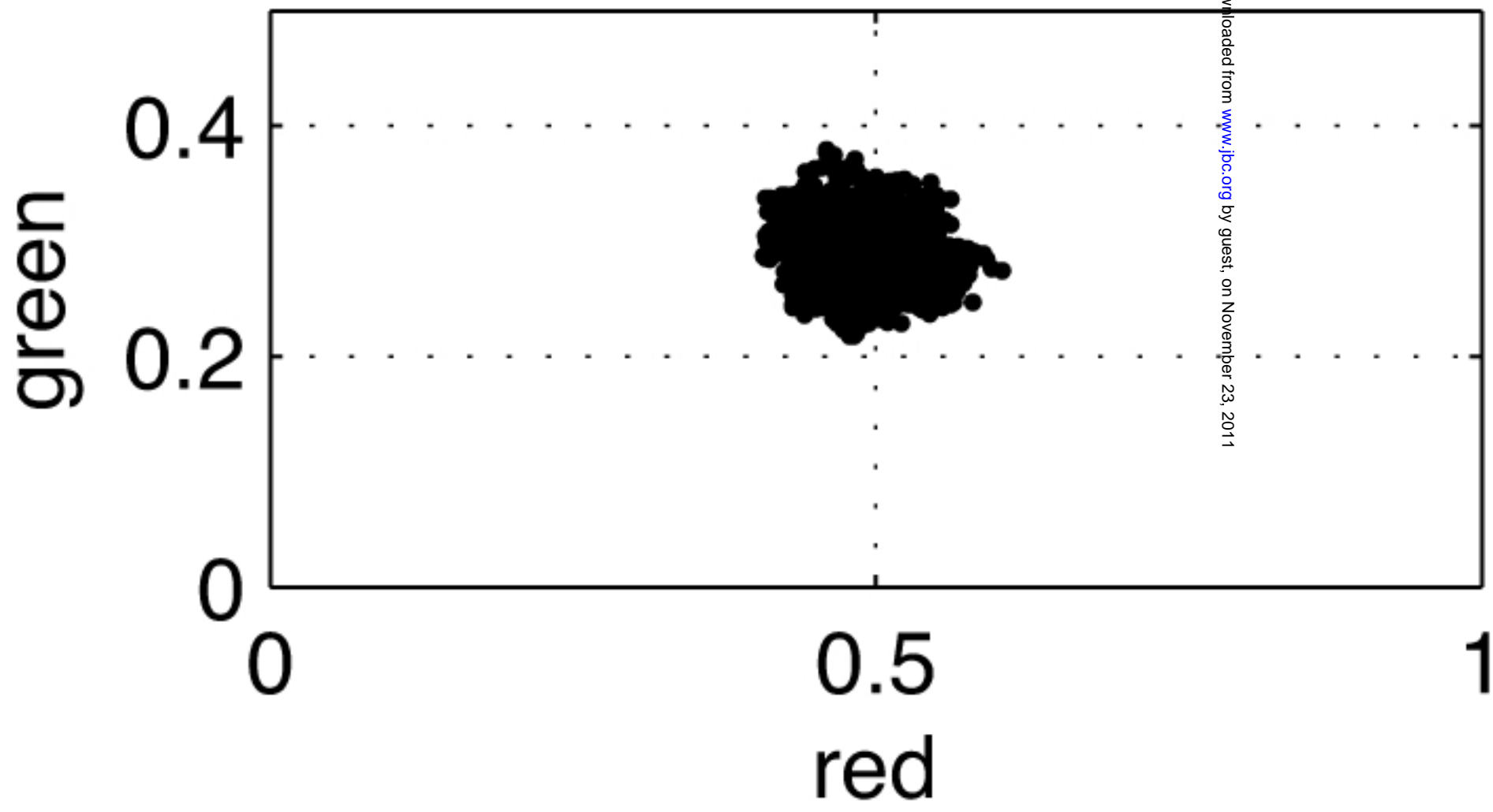
1278 2+ 42 28.300 7.200 58% 2119.0700 +0.6000 0.9107 9

sp|P17661|DESM_HUMAN

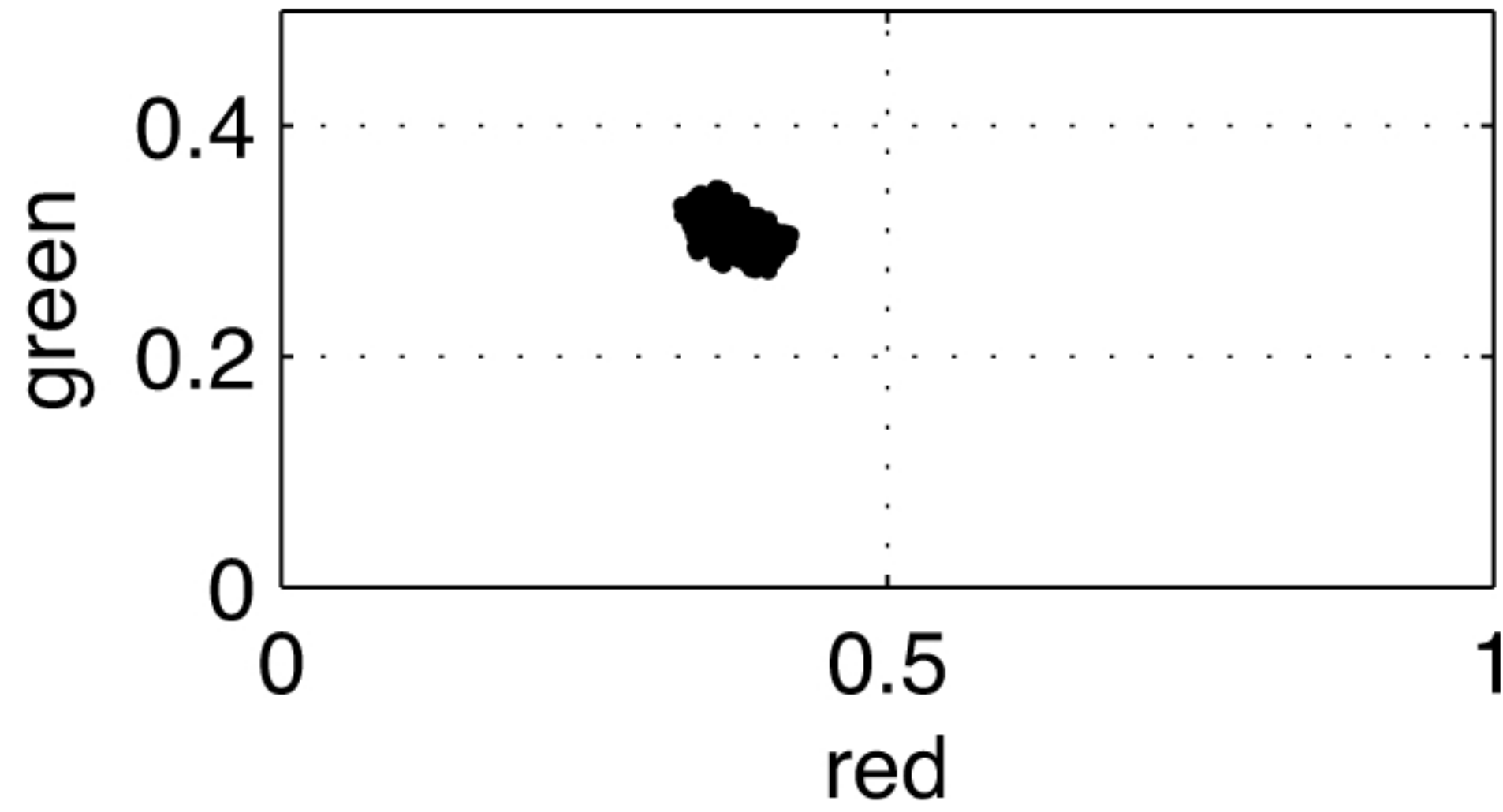


b ²⁺	b ⁺	#	AA	#	y ⁺	y ²⁺
69.5785	138.1490	1	H	14		
133.6438	266.2797	2	Q	13	1982.9880	991.9980
190.2236	379.4392	3	I	12	1854.8572	927.9326
254.2889	507.5699	4	Q	11	1741.6978	871.3529
297.8280	594.6481	5	S	10	1613.5671	807.2875
379.4160	757.8241	6	Y	9	1526.4889	763.7484
429.9685	858.9291	7	T	8	1363.3129	682.1604
716.6729	1432.3379	8	C'	7	1262.2078	631.6079
781.2307	1561.4534	9	E	6	688.7991	344.9035
837.8104	1674.6128	10	I	5	559.6836	280.3458
895.3547	1789.7014	11	D	4	446.5241	223.7660
930.8941	1860.7802	12	A	3	331.4355	166.2217
987.4738	1973.9397	13	L	2	260.3567	130.6823
		14	K	1	147.1973	74.1026

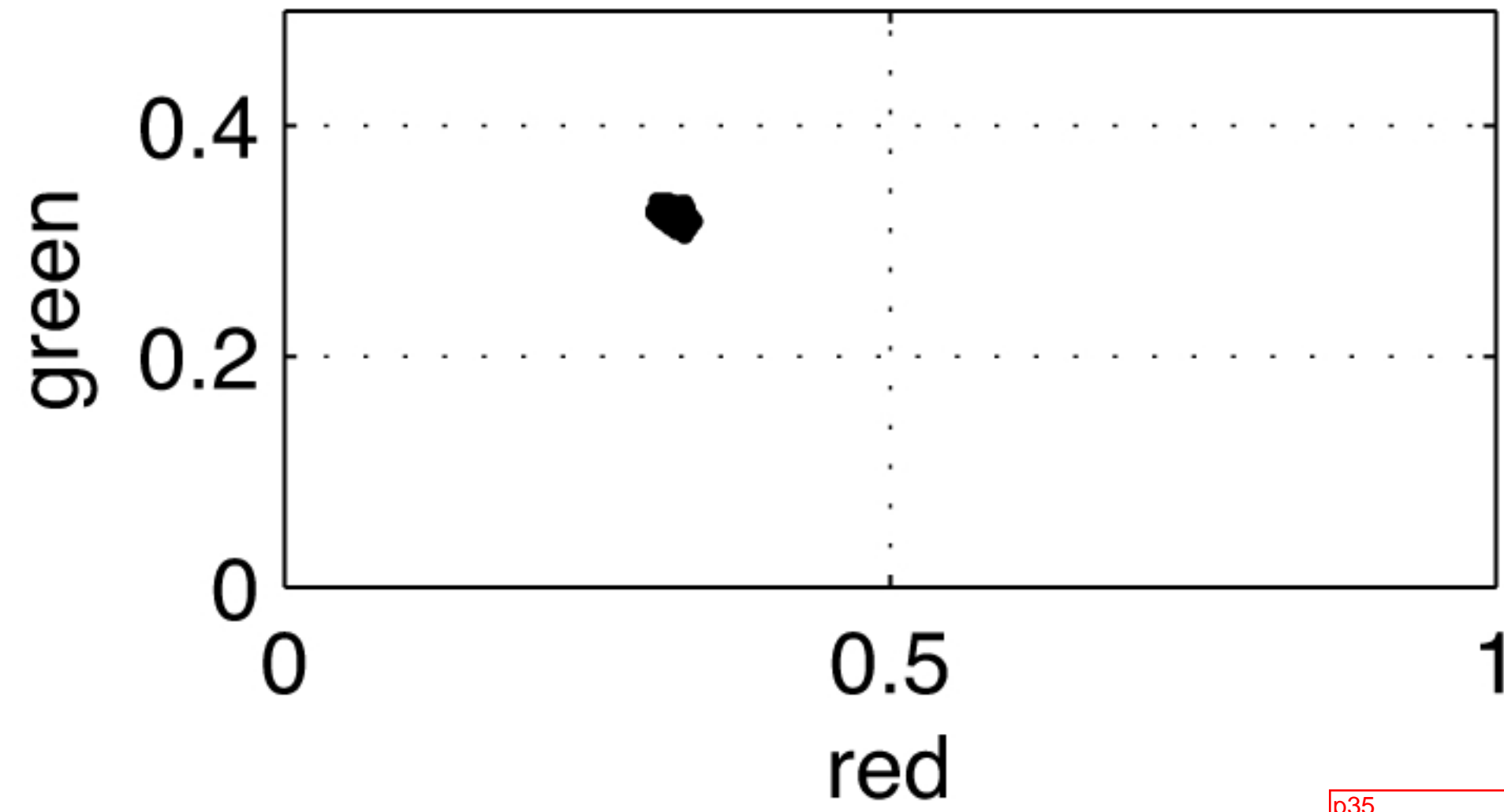
A



B



C



For the purpose of quantitatively evaluating the opacity of the cornea, we note that as corneal opacity increases, the colors of the iris pixels of the camera approach colorless shades of gray. As such, we can rely on color theory and measure the variance in the colorfulness of each pixel. In colorimetry, colorfulness is a measure of how far a specific color is from neutral gray, independent of brightness. The process is characterized by visualizing each pixel of the camera as a point in 3-D space characterize by a red, green, and blue axis where each color component corresponds to a number in the range from 0 to 1. Converting these (red, green, blue)-triplets into a measure of colorfulness is then performed by, first, projecting each point onto a 2-D plane defined by **R** and **G** axes according to the following equations:

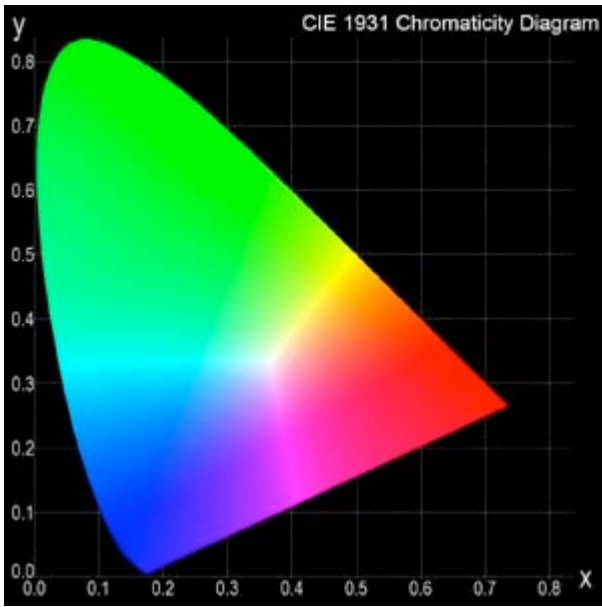
$$r = \text{red} / (\text{red} + \text{green} + \text{blue}) \text{ and}$$

$$g = \text{green} / (\text{red} + \text{green} + \text{blue}).$$

On this plane, shades of gray map to the $(r=1/3, g=1/3)$ coordinate while solid reds, greens, and blues get mapped to the three corners, $(1,0)$, $(0,1)$, and $(0,0)$ respectively, of a color triangle. Repeating this map for each and every pixel within a region of interest from a subject photograph produces a cloud of points on the R, G axis as depicted in Fig. S4, which shows the point clouds produced for three sample images where subject A has the least measure of opacity, indicated by a sparsely distributed point cloud, while subject C has the highest measure of opacity indicated by a tight clustering of points surround the white coordinate. To convert these point clouds into a scalar measure of opacity, we simply measure the mean distance of these colorfulness points from their mean according to:

$$\text{opacity} = \frac{1}{N-1} \sum_{i=1}^N \sqrt{(r_i - \bar{r})^2 + (g_i - \bar{g})^2} \quad 2$$

where r and g represent the mean X and Y coordinates of the cloud.



The CIE 1931 Chromaticity Diagram taken from <http://hancocktechnologies.com/Color%20Basics.html>

Table S1

Computer-assisted Image Clarity Percentile Curve Comparisons

Comparison	A vs B	A vs C	A vs D	B vs C	B vs D	C vs D
P-value	< 0.0001	< 0.0001	< 0.0001	> 0.2368	< 0.0001	0.0096

Human Scored Clarity Percentile Curve Comparisons

Comparison	A vs B	A vs C	A vs D	B vs C	B vs D	C vs D
P-value	< 0.0001	< 0.0001	< 0.0001	> 0.02	> 0.07	> 0.003

A = $Vim^{+/+}$ - Veh; B = $Vim^{+/+}$ - WFA; C = $Vim^{-/-}$ - Veh; D = $Vim^{-/-}$ - WFA